Titanium in GGBS-like calcium-magnesium-aluminosilicate glasses: Its role in the glass network, dissolution at alkaline pH and surface layer formation

Simon Blotevogel, Mathilde Poirier, Delphine Vantelon, Erwan Chesneau, Charles-Emmanuel Dutoit, Valérie Montouillout, Franck Fayon, Judit Kaknics, Gautier Landrot, Giuseppe D. Saldi, et al.

▶ **To cite this version:**

Simon Blotevogel, Mathilde Poirier, Delphine Vantelon, Erwan Chesneau, Charles-Emmanuel Dutoit, et al.. Titanium in GGBS-like calcium-magnesium-aluminosilicate glasses: Its role in the glass network, dissolution at alkaline pH and surface layer formation. Journal of Non-Crystalline Solids, 2022, 591, pp.121708. 10.1016/j.jnoncrysol.2022.121708 . hal-03820235

HAL Id: hal-03820235
https://hal.science/hal-03820235

Submitted on 16 Mar 2023

HAL is a multi-disciplinary open access archive for the deposit and dissemination of scientific research documents, whether they are published or not. The documents may come from teaching and research institutions in France or abroad, or from public or private research centers.

L'archive ouverte pluridisciplinaire **HAL**, est destinée au dépôt et à la diffusion de documents scientifiques de niveau recherche, publiés ou non, émanant des établissements d'enseignement et de recherche français ou étrangers, des laboratoires publics ou privés.

Titanium in ground-granulated blast-furnace slag like calcium-magnesium-aluminosilicate glasses: Its role in the glass network, dissolution at alkaline pH and surface layer formation

Simon Blotevogel[1], Mathilde Poirier[2], Delphine Vantelon[3], Erwan Chesneau[4], Charles-E Dutoit[5], Valérie Montouillout[4], Franck Fayon[4], Judit Kaknics[6], Gautier Landrot[3], Giuseppe D. Saldi[7], Jacques Schott[7], Hervé Vezin[5], Cedric Patapy[1], Martin Cyr[1]

[1] *LMDC, Université de Toulouse, INSA/UPS Génie Civil, 135 Avenue de Rangueil, 31077, Toulouse cedex 04, France*

[2] *Ecocem Materials, 324061, Block F1, Eastpoint Business Park, Dublin 3, Ireland*

[3] *Synchrotron SOLEIL, L'orme des merisiers, Saint Aubin BP48, 91192 Gif sur Yvette cedex, France*

[4] *CNRS CEMHTI UPR3079, 1D av. de la Recherche Scientifique, 45071 Orléans, France*

[5] *Université de Lille, CNRS, UMR8516-LASIRE, F-59000 Lille, France*

[6] *ArcelorMittal Maizieres Research, Voie Romaine, 57283 Maizières-les-Metz, France*

[7] *Géosciences Environnement Toulouse (GET), Observatoire Midi Pyrénées, Université de Toulouse, CNRS, IRD, 14 Avenue E. Belin, 31400 Toulouse, France*

Keywords :

CMAS, supplementary cementitious materials (SCM), gel layer, XAS, cement, coordination, corrosion, non-bridging oxygen

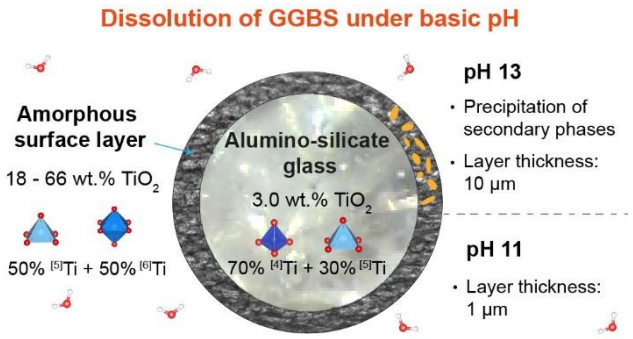

Abstract

Ground-granulated blast-furnace slags (GGBS) are common replacements of Portland cement in low-carbon cements. However, small TiO_2 contents in the slag-glass significantly reduce its cementitious reactivity. Here, we investigate the role of Ti in the glass network and its influence on slag-glass dissolution. XANES and EPR analysis showed that 67% of Ti was present as Ti(IV) with about 70 % in $^{[5]}$Ti and 30 % in $^{[4]}$Ti coordination and 33% as Ti(III). Initial dissolution rates at pH 11 were only slightly decreased (10-28%) by the presence of Ti in model glasses and modified slags, dissolved Si after 7d even less. During dissolution, Ti accumulated in an amorphous layer at the glass surface. At pH 11 the layer was mainly composed of TiO_2 (66 wt.%), whereas it was intermixed with a hydrotalcite-like phase at pH 13. Ti K-edge XANES of the surface layer revealed a change of Ti coordination to 50% of $^{[5]}$Ti and 50% of $^{[6]}$Ti coordination at both pH. Our results suggest that the drastic loss of cementitious reactivity in the presence of Ti is not only due to stabilization of the glass structure by Ti, but also to the formation of a Ti-rich surface layer that may become passivating.

1. Introduction

Ground-granulated blast-furnace slags (GGBS) are calcic-magnesium-aluminosilicate (CMAS) glasses that are by-products from hot metal production. They are used as a cement additive, replacing clinker/Portland cement to up to 95% in some applications. GGBS-containing binders have superior long term properties, compared to traditional cements, including increased chemical and mechanical resistance and decrease the CO_2 footprint of the material.[1–7] During the hydration reaction of blended cements, the vitreous slag dissolves in an alkaline (due to the presence of cement or an activator) aqueous medium. Subsequently, typical cementitious phases as calcium-aluminium-silicate-hydrates (C-(A)-S-H), various layered double hydroxydes, and ettringite, precipitate providing mechanical strength to the material.[2,6,8] Large differences exist in short term reactivity of GGBS depending on its composition.[8,9] These differences can partially be explained by the polymerization degree of

the SiO_2 network that controls dissolution rates and subsequently short-term compressive strength.[8,10–13]

In GGBS glasses, mainly SiO_2 and, to a smaller extent, Al_2O_3 are the principal network formers whereas CaO, together with small amount of MgO, is the main network modifier.[2,6,10,12–14] TiO_2 is present at the level of up to a few weight percent (wt%) in GGBS, but its presence has been reported to have a negative effect starting from 1 wt. % TiO_2 in blended cements.[9,13,15,16] Standard mortars containing 75 % GGBS lost more than 50% of compressive strength after 2 d of curing when 1.9 wt% TiO_2 were added to the slag. The effect was only slightly smaller at 28 d.[9] The loss of reactivity in presence of Ti was recently assigned to a stabilization of the glass network, supposedly resulting in lower dissolution rates.[17]

The Ti coordination environment in glasses and melts has frequently been studied using X-ray absorption near-edge structure (XANES) spectroscopy.[18–21] Information on the coordination environment of Ti is mainly inferred from the position and height of a pre-peak before the K-edge.[20] A recent study on GGBS glasses reported 4- and 5-fold coordinated Ti(IV), with some 25% of Ti in Ti(III) oxidation state.[17] In other alumino-silicate glasses a variety of coordination environments, with coordination numbers ranging from 4 to 6, were reported depending on their non-bridging oxygen per tetrahedron (NBO/T) ratios, Ti content and the presence of Al and large cations.[18,20–22] This variability is interesting as there likely is an impact of Ti-coordination on the rate of glass dissolution.[23]

The dissolution rates of slag-glasses at conditions close to the blended cement environment are difficult to measure because of the low solubility of Mg bearing minerals at pH > 9. Therefore, dissolution studies of slag-like glasses reported in literature used simplified glasses containing only Ca, Al, and Si.[24,25] Snellings et al. (2013) showed that the dissolution of slag-like glasses was stoichiometric at pH 13 and that the presence of Ca and Al in solution, unlike that of Si or SO_4, decreased the dissolution rates.[25] Newlands et al. (2017) measured faster release of Ca in the first minutes of dissolution and slightly higher dissolution rates of Si than Al in slag glasses at pH >12. This led to the formation of a leached surface layer, including re-adsorption of Ca and precipitation of secondary phases.[24] In many

silicate glasses, the formation of a surface layer was reported to decrease the dissolution rates to different extents, depending on its compositionr.[26–28]

Until now no dissolution rates were reported for Ti containing GGBS glasses. However, elements of the IVB group, including Ti, were reported to decrease the dissolution rates of (boro-)silicate glasses. Zr and Ti inhibit corrosion in 0.5M HNO_3 solution and notably decrease network modifier interdiffusion.[29] Furthermore, Ti additions of 4 mol% (ca. 5 wt%) in a borosilicate glass decreased its dissolution rate by about 50% at pH 7.[23] This t is partly due to higher free enthalpy of glass hydration, and thus slower dissolution rates.[23,30–34] Furthermore, it has been noted that Zr and Ti played a role in the densification and pore closure of the gel layer in various experiments.[23,26,35]

In this study, the effect of TiO_2 addition (0-2.5 wt% TiO_2) on GGBS glass structure and dissolution rates under alkaline conditions was investigated. The aim was to determine if the mechanism by which TiO_2 decreases GGBS reactivity is the stabilization of the glass network and consequently decreased dissolution rates, as proposed in literature.[17]Therefore, we performed mixed-flow dissolution experiments of model glass and modified slag samples at pH 11 and 20°C to determine their dissolution rates. The pH value was chosen to be below common cement conditions to prevent the precipitation of Mg-bearing phases. After the dissolution runs the glass surface was analyzed using scanning and transmission electron microscopies (SEM/TEM) to investigate the surface layer. To confirm the surface layer formation also at cement conditions, we conducted SEM analysis of slag grains after ten days of exposure at pH 13. Micro-focused Ti K-edge XANES analyses of the surface layer and the unreacted slag were performed to determine the coordination of Ti. At pH 13 Mg was detected in the surface layer, therefore also the Mg-environment in the GGBS and the surface layer was investigated by Mg K-edge XANES.

2. Materials and Methods

In this study, multiple model glasses (MG) and modified slags (MS), with variable TiO_2 content and Ca/Si ratios were prepared (section 2.1). Not all analysis were carried out on all samples that were prepared for this study (Table 1). Dissolution rate at pH 11 (section 2.2) was investigated during 7 d, on MS with the lowest (MS-Ref) and the highest Ti content (MS-Ti-2.4) and model glasses with and without Ti addition, except MG-Ti-oxi and MG-Ti-red. This

pH was chosen to be below the pH of typical cement environments to avoid supersaturation of Mg-bearing minerals. For these experiments powdered samples were sieved and the fraction between 40 and 80 µm was used. The samples were chosen to have large differences in Ti contents and NBO/T to improve detection of effects on dissolution rate. For surface analysis after dissolution at pH 11, including SEM, TEM and Ti- (section 2.4) and Mg µ-XANES (section 2.5), 250 mg of a MG-1.2-Ti sample was dissolved for 14 d.

To investigate the surface layer formation at a pH closer to the cement environment and still avoid oversaturation of Mg-bearing minerals, dissolution experiments at pH 13 were carried out on Ti-bearing, granulated samples (section 2.3): the MS sample with the highest Ti content (MS-Ti-2.4) and the two Ti bearing MGs (MG-1.2-Ti and MG-0.8-Ti). After the dissolution experiment the surface layer formation was investigated by SEM and Ti k-edge µ-XANES on polished section. In those samples, XANES spectra of intact slag were recorded in the core of the reacted samples using the micro-focused beamline setup (section 2.5). To check for differences between powdered and polished sample presentation, a powdered MS-Ti-2.4 sample was also measured in this setup.

To investigate the Ti-environment in close to real slag-glasses, powder XANES analysis (section 2.5) was carried on unreacted powders of all MS samples as well as on MGs produced under oxidizing and reducing atmosphere (MG-Ti-oxi and MG-Ti-red). The latter were used to study the influence of the presences of Ti(III) on the XANES signal, therefore those were the only samples analyzed by EPR (section 2.4).

Table 1. Overview of analysis carried out on each sample.

ID	Dissolution pH 11	SEM/TEM after pH 11	µ-XANES (Ti) after pH 11	SEM after pH 13	µ-XANES (Ti) after pH 13	µ-XANES (Mg) after pH 13	XANES (Ti) powders	EPR
MS-Ref	x						x	
MS-Ti-1.6							x	
MS-Ti-2.4	x			x	x		x	
MG-1.2-Ti	x	x	x	x	x	x	x	
MG-1.2-NoTi	x							
MG-0.8-Ti	x			x	x			
MG-0.8-NoTi	x							
MG-Ti-red							x	x
MG-Ti-oxi							x	x

2.1 Preparation of model glasses and modified slags

Model Glasses (MG) were prepared by mixing pure reagents. SiO_2 was added as Fontainebleau sand (VWR), XRF analyses showed that oxides other than SiO_2 were below 0.1 wt%. CaO, MgO and Al_2O_3 were also purchased from VWR. To eliminate possible carbonation products, CaO and MgO powders were calcined at 1100 °C in Pt-crucibles before use. The TiO_2 powder was purchased from Rectapur (purity >98 % (m/m)). Modified Slag (MS) samples were prepared by mixing an industrial GGBS (produced by ArcelorMittal, and ground/commercialized by Ecocem Materials), with TiO_2 powder. The remelting procedure was the same as for the model glasses.

Oxides mixtures of fixed compositions were placed in a graphite crucible in a Nabertherm HT16/17 furnace preheated at 1600 °C. The furnace was purged with argon to limit interaction of air with the graphite crucible. Once the temperature stabilized to 1600 °C (temperature drop due to cooling effect of cold crucible), the samples were kept for 5 minutes to ensure complete melting. The samples were taken out of the furnace at 1600 °C with a pair of pliers and quenched in a laboratory scale granulation device using pressurized water flow. The recovered granulated slags were dried overnight at 110 °C. The amorphous state of the samples was checked by XRD on powdered samples (supplementary information (SI), Figure SI-1).

Six different MG were prepared: A set of two glasses with a Ca/Si molar ratio of 1.2 with (MG-1.2-Ti) and without Ti addition (MG-1.2-NoTi). A second set of model glasses was synthesized with a Ca/Si molar ratio of 0.8, again with (MG-0.8-Ti) and without TiO_2 addition (MG-0.8-NoTi). The Ca/Si ratio of 1.2 is a typical value for GGBS, and the lower Ca/Si ratio of 0.8 was chosen to be comparable to other CMAS glasses reported in literature. Finally, a set of two model glasses with a Ca/Si molar ratio of 1.1, was prepared to study the effect of reduced and oxidizing conditions. MG-Ti-red was prepared like the other model glasses under reducing conditions, whereas for MG-Ti-oxi a Pt-Rh crucible was used and the oven was not Ar-purged.

Besides, four MS-samples with increasing TiO_2 amounts were prepared: MS-TiO_2-1.1 (1.1 wt% TiO_2), MS-TiO_2-1.6 (1.6 wt% TiO_2), MS-TiO_2-2.0 (2.0 wt% TiO_2) and MS-TiO_2-2.4 (2.4 wt% TiO_2). As a reference (MS-Ref), an industrial slag sample was remelted using the same

procedure but without any Ti addition. The exact compositions determined by XRF of the final glass powders are displayed in Table 2, along with Ca/Si and Al/Si molar ratios.

The NBO/T ratio was estimated from composition of non-Ti bearing glasses, using the formula (1). Therefore, structural hypothesis need to be made for the elements that were taken into account. Ca and Mg were accounted for as network modifying cations contribution 2 charges each, whereas Si was accounted for as network former, contributing one tetrahedron per atom, in line with literature.[14,36,37] The case of Al is more difficult as it can occur in different coordination states in different glasses.[38–40] All glasses investigated here are in the peralkaline region, so that Al is expected to be in tetrahedral coordination.[40] This is supported by experimental results on GGBS glasses that reported the large majority of Al in 4-coordinate positions.[10,14] In tetrahedral coordination, Al contributes one tetrahedron per atom, but also requires charge compensation due to its 3+ oxidation state. Ti was not included in NBO/T calculation here, because the necessary structural hypothesis will be experimentally examined in this study and discussed below.

$$\frac{\mathrm{NBO}}{\mathrm{T}} = \frac{2\mathrm{n_{Ca}} + 2\mathrm{n_{Mg}} - \mathrm{n_{Al}}}{\mathrm{n_{Si}} + \mathrm{n_{Al}}} \qquad (1)$$

Table 2. XRF analysis of modified slags and model glasses. Elemental ratios are given as molar ratios and NBO/T was calculated for glasses not containing Ti.

ID	Type of GGBS	Al_2O_3 wt. %	CaO wt. %	MgO wt. %	SiO_2 wt. %	TiO_2 wt. %	Ca/Si mol/mol	Al/Si mol/mol	NBO/T
MS-Ref	Modified slag	9.8	42.4	6.9	37.9	0.7	1.21	0.31	
MS-Ti-1.6	Modified slag	9.7	42.4	6.8	37.8	1.6	1.21	0.31	
MS-Ti-2.4	Modified slag	9.6	41.8	6.8	37.4	2.4	1.21	0.31	
MG-1.2-Ti	Model glass	11.2	40.4	7.1	37.7	3.1	1.16	0.36	
MG-1.2-NoTi	Model glass	11.6	41.7	7.3	39.0	-	1.16	0.36	1.86
MG-0.8-Ti	Model glass	11.1	32.7	7.0	45.6	3.1	0.78	0.29	
MG-0.8-NoTi	Model glass	11.5	33.8	7.2	47.1	-	0.78	0.29	1.33
MG-Ti-red	Model glass	11.3	39.5	7.0	39.0	3.1	1.10	0.35	
MG-Ti-oxi	Model glass	11.3	40.0	7.1	38.3	3.1	1.13	0.35	

2.2 Dissolution runs on powdered samples at pH 11

2.2.1 Experimental design

Dissolution experiments at pH 11 were carried out in mixed-flow reactors. Subsamples of 15 g of granulated slag were ground for 15 s in a disc mill by Retsch. The resulting powders were sieved and the fraction between 40 and 80 µm was retained. The powdered samples were subsequently suspended in acetone and exposed to an ultrasound treatment for 20 s, after which the supernatant acetone was taken off to eliminate adhering small particles from the powders. After acetone treatment, the samples were vacuum dried. The particle size distribution (PSD) curves are similar enough to consider the same reactive surface for all the samples (Figure SI-2).

Dissolution runs were carried out using custom made 250 mL polypropylene reactors at 25°C with a continuous flow of about 2.0 mL/min using a peristaltic pump. To promote mixing of the solution and to avoid particle loss through the outflow, the inflow was situated at the bottom and the outflow at the top of the reactor. The solutions were stirred at 100 rpm using a floating magnetic stirrer. A 80 mg subsample was put into the reactors and exposed to a NaOH solution at pH 11 for 7 days. The experimental conditions (pH, sample mass, grain size, flow rate) were chosen to keep the reacting solution undersaturated with respect to Mg-bearing phases during the experiment, and at the same time to be able to measure dissolved Ca, Mg, Al and Si by ICP-OES. Dissolution of a MG-1.2-NoTi sample was replicated with 25% lower flow rate to estimate experimental error and to evaluate if calculated dissolution rates were independent of flow rate/reactive surface ratios so that far-from equilibrium conditions can be assumed.

2.2.2 Analysis of mixed-flow solutions

During the dissolution experiment, a 20 mL solution sample was taken at the outflow of the reactors twice a day. Exact flow rate was determined by weighing and pH was checked to be constant within experimental uncertainty. The solutions were immediately filtered at 0.45 µm. Before chemical analyses, solutions were acidified to 2 vol.% HNO_3 and spiked with Y as an internal standard at 1 mg/L. Concentrations of Ca, Mg, Al, Si and Ti were analyzed by ICP-OES (Optima 7000, by Perkin Elmer). Internal precision was checked by measuring blank and reference solutions every 20 samples. Quantification limits calculated as mean plus 10 x standard deviation of analytical blanks (n=33, for Si n=28) were 23, 3, 9, 16 and 0.4 µg/L, respectively for Ca, Mg, Al, Si and Ti. Analytical precision calculated as two standard

deviation interval around the mean of 0.1 mg/L (0.2 mg/L for Si) internal standard (n=13, for Si n=15) were ±14, ±2, ±3, ±7 and ±3 µg/L, respectively for Ca, Mg, Al, Si and Ti. Fluctuations of plasma intensity were corrected for by analyzing an internal standard. If the internal standard concentration differed by more than 10 % from the spiked concentration, the measurement was repeated.

2.2.3 Reacted surface analysis

For the investigation of the reacted glass surface after dissolution at pH 11, a 250 mg MG-1.2-Ti sample was reacted under the conditions described in section 2.2.2 for 14 days. After 14 days the remaining powder was immersed in 100 mL of isopropanol for 10 min in order to stop the reaction and extract any remaining water. The sample was then filtered off, rinsed with acetone and vacuum-dried.

The surface of reacted grains was analyzed using a FEI Helios NanoLab600i dual beam SEM-FIB equipped with an Aztec Advanced SDD X-Max 80 mm² EDS detector at the Centre Raymond Castaing, Toulouse, France. Subsequently, a vertical slice for TEM analysis was cut using a Ga-ion beam and lifted out by an EasyLift micromanipulator. For the TEM slice preparation, the ion column was operated at 30 kV for all the steps, except for final cleaning of the specimen, for which tensions of 5 kV and 2 kV were used. The beam currents varied between 47 nA and 15 pA. The electron beam was used to deposit a 20 nm thick carbon layer over an area of 20 µm x 2 µm. The ion beam was then used to deposit a 3 µm thick Pt layer over the same area. The slice was partially cut out and a Pt needle was fixed. The sample was lifted out in situ and then attached to a copper support grid. Thinning of the specimen could then proceed using a gradual cross-section cleaning milling pattern, with a final milling beam current of 80 pA. Finally, the 5 kV and 2 kV cleaning steps were carried out on each side. TEM images were acquired with a JEOL 2100F TEM. The electron gun is a Schottky emitter used with a voltage of 200 kV. The slice was observed with a Gatan Ultrascan Camera in transmission and diffraction modes. The EDS spectrum and mapping used a Bruker SDD. All the STEM images were done using a HAADF STEM detector.

2.3 Dissolution trials on granulated glasses at pH 13

2.3.1 Experimental design

To investigate surface layer formation of modified slags and model glasses at a pH close to that of cement pore solutions, 300 mg of three Ti-containing granulated samples (MG-1.2-Ti, MG-0.8-Ti and MS-Ti-2.5) were partly dissolved by circulating a NaOH solution at pH 13 for 10 days. Dissolution trials were carried out using the mixed-flow reactors described in section 2.2. The granulated sample form was chosen to reduce the reactive surface and to avoid oversaturation.

2.3.2 Sample preparation

After 10 days the remaining granules were immersed in 100 mL isopropanol for 10 min to extract any remaining water. Subsequently, isopropanol solution was filtered off and the samples were rinsed with acetone and vacuum dried. The three granulated slag samples were then put into 20 g of MA2+ resin using 2.5 g of 100 CC catalyst (by Presi). After one night of hardening, sample sections were polished to obtain grain cross sections, using three successive SiC papers of 800, 1200 and 2400 grits.

2.3.3 Reacted surface analysis

All samples were stored under vacuum until Scanning Electron Microscopy (SEM) analyses. Images and elemental maps were carried out at the LMDC laboratory (France) using a JEOL JSM 6380 equipped with an Energy-Dispersive Spectrometer (EDS). The analyses were conducted on the three polished cross-sections samples described in section 2.3.1. Before analysis, the samples were carbon-coated. The SEM images were taken in back-scattered electron mode using an acceleration voltage of 15 keV. Elemental maps of Al, Si, Mg, Ca and Ti were collected using 5 cycles of 500 s.

2.4 EPR analysis

The redox state of Ti in unreacted powdered slag glass samples was investigated by Electron Paramagnetic Resonance (EPR) spectroscopy at the LASIRE laboratory in Lille, France. All samples were inserted into quartz Suprazil tubes. Continuous wave EPR (cw-EPR)

measurements were performed at room temperature on a conventional X-band Bruker ELEXSYS E580 spectrometer operating at 9.8 GHz. The modulation frequency was set at 100 kHz and its amplitude was chosen at 0.5mT for MG-TI-red and MG-Ti-oxi to prevent distortion due to over-modulation . The microwave power into the resonator was set at 4 mW (MG-Ti-red) and 0.6 mW (MG-Ti-oxi) in order to avoid saturation of the EPR line. A small amount of TiF_3 was used as reference to estimate the amount of Ti(III) species for each sample.

2.5 Ti K-edge XANES experiments

To investigate the coordination number (CN) of Ti in slag glasses and alteration layers, two sessions of Ti K-edge XANES experiments were carried out at the SOLEIL synchrotron facility in Saint-Aubin (France) using the SAMBA and LUCIA beamlines. Details on the influence of monochromator type and beamline setup on the pre-edge features can be found in the supporting information (Figure SI-3).

2.5.1 Bulk powder analysis at SAMBA beamline

During the SAMBA session, three unreacted powdered modified slag samples (MS-Ref, MS-Ti-1.6 and MS-Ti-2.5), as well as two unreacted powdered model glass samples prepared under reducing (MG-Ti-red) or oxidizing conditions (MG-Ti-oxi), were studied. Pure samples of rutile (r-TiO_2, 99.8%), anatase (a-TiO_2, 99.6%), and tistarite (Ti_2O_3, 99.8%) were used as reference compounds, their XRD patterns are shown in the supporting information (Figure SI-4). All samples were pressed into metaborate pellets containing 1 wt% TiO_2. The monochromatic beam, which was delivered by a Si(220) double-crystal monochromator, was calibrated at the Ti K-edge, using a Ti foil. Data were acquired in fluorescence mode (FY) for the GGBS samples, using a 33 pixel fluorescence Ge detector (Canberra), and transmission mode for the reference materials. Samples were orientated at 90° and 45° to the incident beam to collect data in transmission and fluorescence mode, respectively. The XANES spectra were recorded in a spectral range of 4850-5349 eV, using a step of 0.2 eV, and 20 scans were recorded for each sample.

2.5.2 Micro-focused analysis of reacted samples at LUCIA beamline

During the LUCIA session, three reacted granulated slag samples (MS-Ti-2.5, MG-1.2-Ti and MG-0.8-Ti) as well as one reacted powdered sample (MG-1.2-Ti (powder)) were studied (see sections 2.2 and 2.3 for details on sample preparation). The samples were fixed on copper mounts using self-adhesives for the granulated slags, and carbon tape for the slag powder. The same three mineral references as in SAMBA (r-TiO_2, a-TiO_2, Ti_2O_3) were measured for quality control. The latter were prepared in cellulose pellets using 10 % TiO_2. All XANES spectra were acquired in fluorescence-mode using a Si-(111) double-crystal monochromator. The beamline was calibrated at the Cr K-edge. The samples were placed in an angle of 80° with respect to the incident beam, and 10° in relation to the 60 mm^2 SDD detector (Bruker). Before spectra acquisition, fluorescence maps of the polished cross-sections were acquired in order to target specific areas in the slag cores (unreacted area) and surfaces (reacted area). The elemental maps were recorded using a micro-beam of 3.3 x 3.6 µm, a step of 2-3 µm and an exposure time of 200 ms. XANES spectra were collected on an energy range of 4850-5200 eV, using a counting time of 2 sec and a step of 2 eV at 4850 eV-4950 eV, 0.2 eV at 4950.2-4990 eV, 0.5 eV at 4990.5-5030 eV and 1 eV at 5031-5200 eV. One to four spectra were collected during each analysis.

2.5.3 XAS data treatment

XANES spectra were averaged and normalized using the Athena software.[41] The normalization parameters were kept as identical as possible between all samples. The absorption threshold E_0 was set to 4982.5 eV, which corresponds to the maximum intensity of the 2nd inflection of the 1st derivative in the GGBS spectra. The spectra were normalized in absorbance by fitting at least the first 40 eV before the pre-edge peak, and by subtracting them as background. Subtraction of atomic absorption was performed by fitting a polynomial line in the middle of the first main post-edge features.

Extraction of the pre-edge peak features (position, normalized height) was done using the Fityk 1.3.1 software. Different methods were reported in the literature to extract the Ti coordination of various silicate glasses and GGBS samples. All of them were based on a nearly identical procedure, which used one lineshape to fit the pre-edge peak, and one to several lineshapes to fit the post-edge features. Among these methods, Farges et al. (1996) reported the use of 6 lorentzian functions to fit the 4960-5020 eV region of various Ti silicate

glasses;[20] Cormier et al. (2011) used 2 lorentzian functions to fit the 4962-4975 eV region of MgO-SiO_2-Al_2O_3-SiO_2-TiO_2 glasses;[42] Romano et al. (2000) used 1 pseudo-voigt function, 1 arctangent function and 2 gaussian lines to fit the 4950-5020 eV region of TiO_2-Al_2O_3-K_2O-SiO_2 glasses,[21] and Le Cornec et al. (2020) used 1 lorentzian function after removing an arctangent function to fit a region (not specified) of various anhydrous industrial slags.[17] All were tested, and gave variations of ± 0.07 eV in position and ± 0.02 a.u in intensity.

In the present study, a variant of the methodology of Romano et al. (2000) was applied.[21] The energy range between 4050-5020 eV was fitted using an arctangent function to model the absorption edge, two gaussian lines to fit the first two main edge features, a single gaussian line to fit the small shoulder in the absorption edge, and a lorentzian function to fit the pre-edge peak. In the case of the mineral references, the pre-edge region was composed of three peaks labelled A1, A2 and A3, so three Lorentzian functions were used for the fitting. The position and normalized height of the pre-edge peak were then extracted from the A2 peak.

2.6 Mg K-edge XANES experiments

Mg K-edge experiments were performed on the LUCIA beamline at the SOLEIL synchrotron facility (Gif-sur-Yvette, France). The beamline was calibrated at the Al K-edge. Analyses were carried out on the granulated slag MG-1.2-Ti. The sample surface was placed in an angle of 60° with respect to the incident beam, and 30° in relation to the 60 mm^2 SDD detector (Bruker). All XANES spectra were acquired in FY mode, using a KTP monochromator. The beam was focused down to 6 × 22 μm^2. XANES spectra were collected on an energy range of 1250-1400 eV, using a counting time of 5 sec and energy steps of 2 eV between 1250-1300 eV, 0.2 eV between 1300.2-1320 eV, 0.5 eV between 1320.5-1340 eV, and 1 eV between 1341-1400 eV. Two spectra were collected both in the slag core and reacted surface, and then averaged using the Athena software. The absorption threshold E_0 was fixed to 1307.6 eV for the slag core, and 1309.5 eV for the reacted layer. These values correspond to the maximum intensity of the first inflection of the 1^{st} derivative of the XANES spectra.

3. Results

3.1 Dissolution of slag glasses at pH 11

3.1.1 Dissolved rates

The amount (wt %) of Si released as a function of time is shown in Figure 1. The more polymerized model glasses MG-0.8-NoTi and MG-0.8-Ti (NBO/T ~1.3) released much less Si (11.5 % and 8.6 % of Si, respectively) than MG-1.2-NoTi and MG-1.2-Ti (NBO/T~1.9; 49.3 % and 48.8 % of released Si, respectively), during the 7 d of the experiment. Note that the value for MG-1.2-NoTi is an average of two independent runs with different flow rates (1.8 and 2.0 mL/min). There was no systematic differences in Si releases that could be linked to modifications of flow rates between the two runs. Therefore, only one dissolution regime at far-from-equilibrium conditions can be assumed. Method error was estimated as the 2 standard deviation (2 SD) interval around the mean from these two runs.

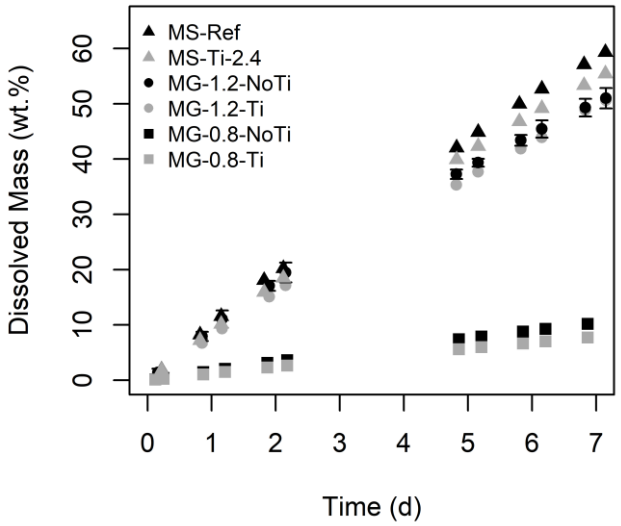

Figure 1. Dissolved mass of the initial glass calculated from Si solution concentration during the pH 11 mixed-flow dissolution experiment for modified slags (MS) and model glasses (MG) with and without Ti addition. Data for MG-1.2-NoTi are averaged from two independent runs with different flow rates and error bars correspond to a two standard deviation interval around the mean.

Modified slags (MS-Ref and MS-Ti-2.4) with slightly higher Ca/Si and slightly lower Al/Si ratio dissolved somewhat more during the 7d experiment than the MG-1.2 samples (57.1 % and 53.3 % of Si for MS without and with Ti addition, respectively). There is a tendency for stronger dissolution of glasses that do not contain Ti. However, if the 2 SD interval is assumed as the method error, this observation was only significant for the modified slags.

The mean dissolution rate of MS-Ref samples, during the first 2 days was 1.49 x 10^{-6} mol(glass).s^{-1}.m^{-2} if a spherical grain shape with a mean radius of 30 µm and congruent dissolution was assumed. Dissolution rates for the other samples shown in Table 3. Calculated dissolution rates during the first 2 days follow the same logic as the dissolved masses after 7 days, described above. Initial calculated dissolution rates were about 17% higher in MS-Ref compared to MG-1.2-No-Ti and a factor x 6 higher than in MG-0.8-NoTi. Dissolution rates of Ti bearing MS-Ti-2.4 was 10 % below MS-Ref and MG-1.2-Ti dissolved 12 % slower than MG-1.2-NoTi, during the first 2 days. Dissolution rate of MG-0.8-Ti was even 28 % below that of MG-0.8-NoTi.

Table 3. Mean dissolution rates during the first 2 d of the experiment, based on Si measurments in solution assuming stoechimetric dissolution and using geometric surface are. The surface area was calculated assuming a spheric grain shape with 30 µm diameter. The method error was estimated as 2 standard deviation interval around the mean of two independent runs of MG-1.2-NoTi at different flow rates.

ID	R $mol_{glass}.s^{-1}.m^{-2}$	log (R)
MS-Ref	1.55E-06	-5.81
MS-Ti-2.4	1.39E-06	-5.86
MG-1.2-Ti	1.16E-06	-5.94
MG-1.2-NoTi	1.32E-06 ± 0.012	-5.88
MG-0.8-Ti	1.87E-07	-6.73
MG-0.8-NoTi	2.60E-07	-6.59

Ca-release during the 7 d experiment was similar to Si so that stoichiometric Ca release relative to Si be assumed (Figure SI-5). However, for some samples, Mg and Al dissolved slightly less than what would be expected for congruent dissolution (Figure SI-5). This

observation may result from minor precipitation of Mg and Al-bearing phases such as hydrotalcite, due to the low solubility of Mg-bearing minerals at high pH. Ti could not be detected in solution although its stoichiometric dissolution should have led to aqueous concentrations largely above its ICP-OES detection limit, thus suggesting its non-stoichiometric release.

3.1.2 Grain surface analysis by SEM/TEM of powders after pH 11 experiments

SEM observation of MG-1.2-Ti powders that were exposed to a NaOH solution at pH 11 for 14 d showed a cracked Ti-bearing layer on the surface of the grains (Figure 2). The layer was about 1 µm thick and in some places covered with small tripod-like objects. The latter may indicate precipitation of secondary minerals as a higher sample mass (250 mg) was used than in the dissolution experiments at pH 11, reported above. EDS analysis of the surface layer showed Ti concentration of 44.6 wt.% TiO_2 (Figure 2, Point 1), against 4.5 wt.% TiO_2 in the crack (Figure 2, Point 2).

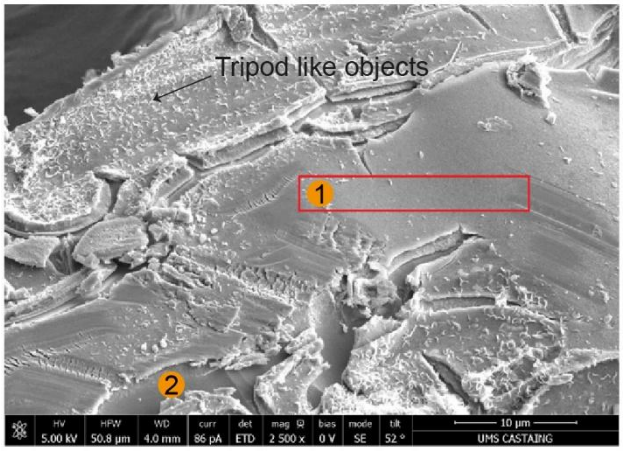

Figure 2. SEM surface analysis (x2500) of MG-1.2-Ti powders after 14 d exposure to a NaOH solution at pH 11. A cracked Ti-bearing layer covers the grain surfaces. The red rectangle indicates the site where the vertical slice for TEM analysis was extracted. Numbers indicate the spots on the surface layer and in the crack where EDS analysis was performed.

The Ti-bearing surface layer was further investigated by extracting a vertical slice for TEM analysis. Analysis of this slice confirmed a thickness of 1 µm and showed that the layer was mainly composed of Ti-oxide. EDS analysis resulted in about 66 wt.% TiO_2, 20 wt.% CaO, 8 wt.% SiO_2, 4 wt.% MgO and 3 wt.% Al_2O_3 (Figure 3). Electron diffraction analysis showed that the surface layer had no regular crystalline structure and can thus be considered as amorphous (Figure 3). Beside the Ti-surface layer there was a few nm thick zone at the glass surface that was enriched in Si and depleted in all other elements (Figure SI-6).

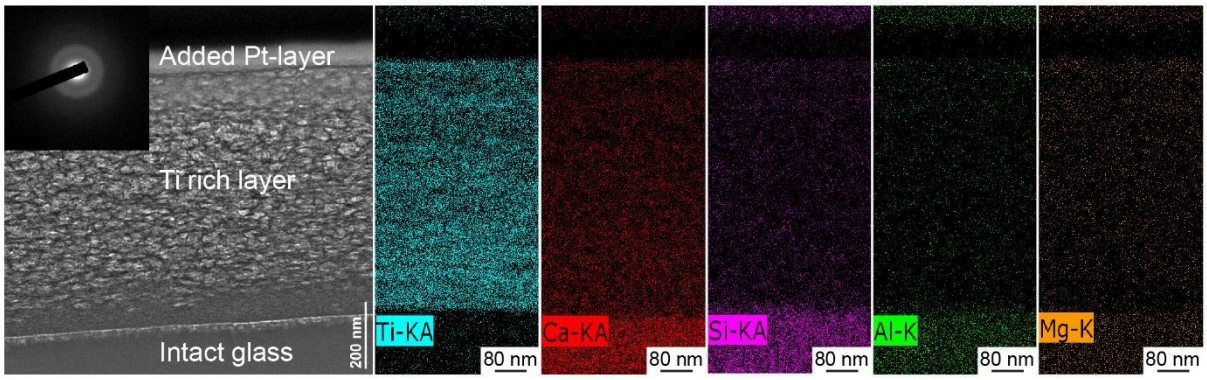

Figure 3: TEM image and EDS maps of the Ti-rich layer extracted from the powder by FIB. The layer is about 1 µm thick and mainly composed of TiO_2 (66 wt.%). The electron diffraction image on the top left indicates that the layer is amorphous.

3.2 SEM observations of grain cross-sections after 10 d at pH 13

SEM images and chemical maps of Si, Ca, Al, Ti, and Mg of slag grains (MG-1.2-Ti, MG-0.8-Ti and MG-Ti-2.5) after 10 d exposure to pH 13 are displayed in Figure 4. The images show a surface layer of about 10 µm thickness, which is enriched in Ti and Mg and depleted in Si, Ca, and Al, compared to the intact glass. The layer was 10 times thicker than in the TEM analysis after pH 11 dissolution and contained Ti, Mg and Al. This is probably related to the pH of 13, which leads to increased dissolution of slag grains and decreased solubility of Mg-bearing minerals. In MG-0.8-Ti, the surface layer was however thinner (from 3 to 10 µm) and not present on all grains. This might be due to the lower dissolution rates of this more polymerized glass. Small nodules of SiO_2 of about 5 µm were also observed in all samples.

Figure 5 shows the evolution of the chemical composition of MS-Ti-2.5 from the core (unreacted area) to the surface (reacted area) of a slag grain. On average, the concentration increased from 9.3 to 16.1 wt.% in Al_2O_3, 6.3 to 37.6 wt.% in MgO, and 2.6 to 18.3 wt.% in TiO_2, and decreased from 44.6 to 10.3 wt.% in CaO and 36.2 to 13.3 wt.% in SiO_2 from the core to its surface. This corresponds to an enrichment by a factor 7 in Ti, 6 in Mg, and almost 2 in Al, and to a depletion by a factor 4 in Ca and almost 3 in Si in the surface layer. Mg and Al were present in a molar ratio of 3:1 suggests and electron backscattered diffraction (EBSD) measurements carried out on an industrial slag show that the surface layer is amorphous to electron diffraction, even in the presence of Mg (Figure SI-7).

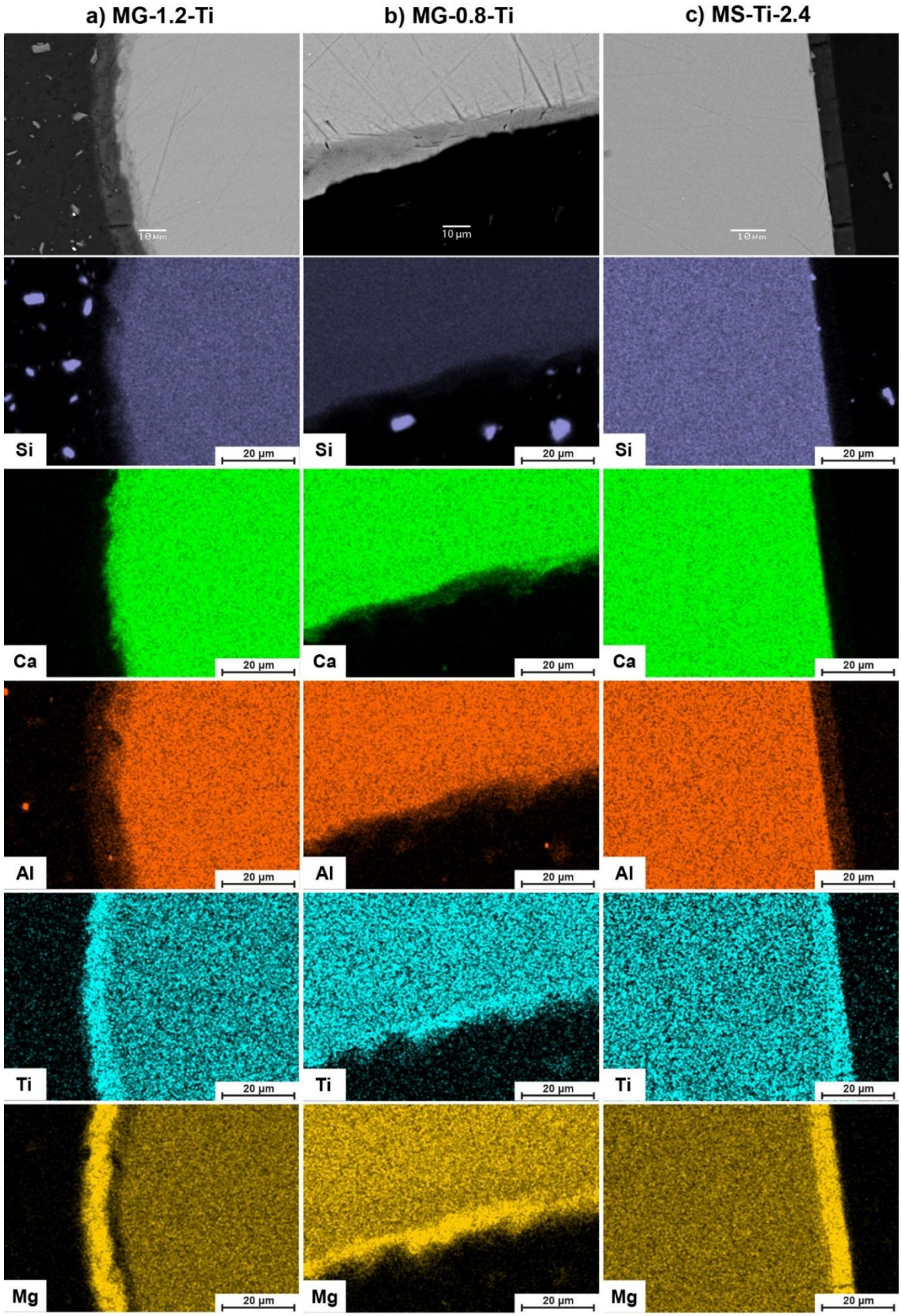

Figure 4: SEM images and elemental maps of Si, Ca, Al, Ti and Mg in the granulated slags of a) MG-1.2-Ti, b) MG-0.8-Ti and c) MS-Ti-2.5, after 10 d exposure to a pH 13 solution.

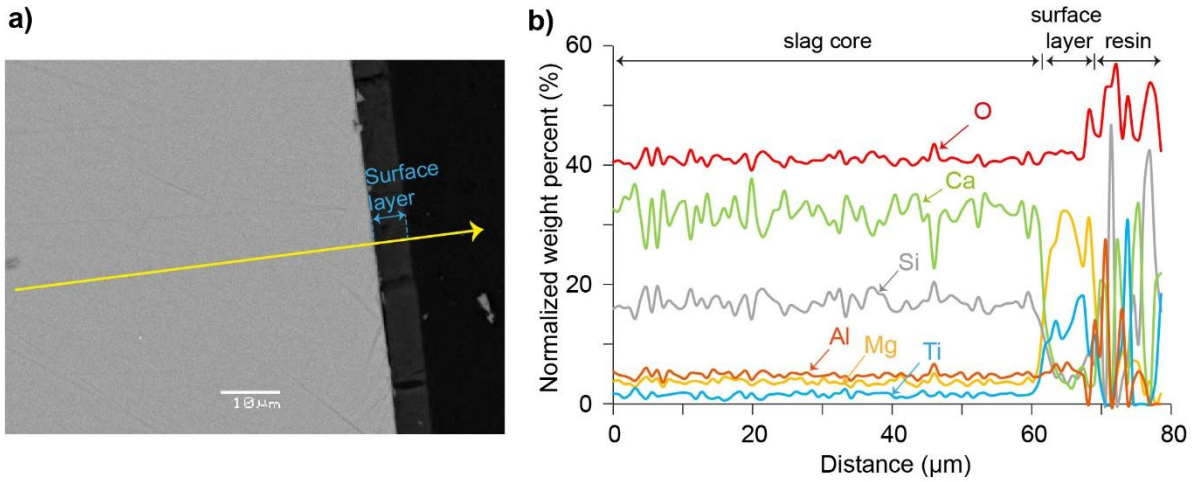

Figure 5: a) Scanning line from the core to the surface of MS-Ti-2.5 after 10 d exposure to pH 13 b) Corresponding elemental distribution in O, Ca, Si, Al, Mg and Ti.

3.3 Ti K-edge XANES measurements

3.3.1 Ti K-edge XANES analysis on bulk powder samples (SAMBA)

The slag-glass spectra (Figure 6a) were composed of three major peaks located at around 4970 eV (pre-edge peak A), 4986 eV (peak B) and 4998 eV (peak C). Due to the absence of a long-range order, only few distinguishable features appeared after peak C in slag-glass samples, in contrast to the mineral references.

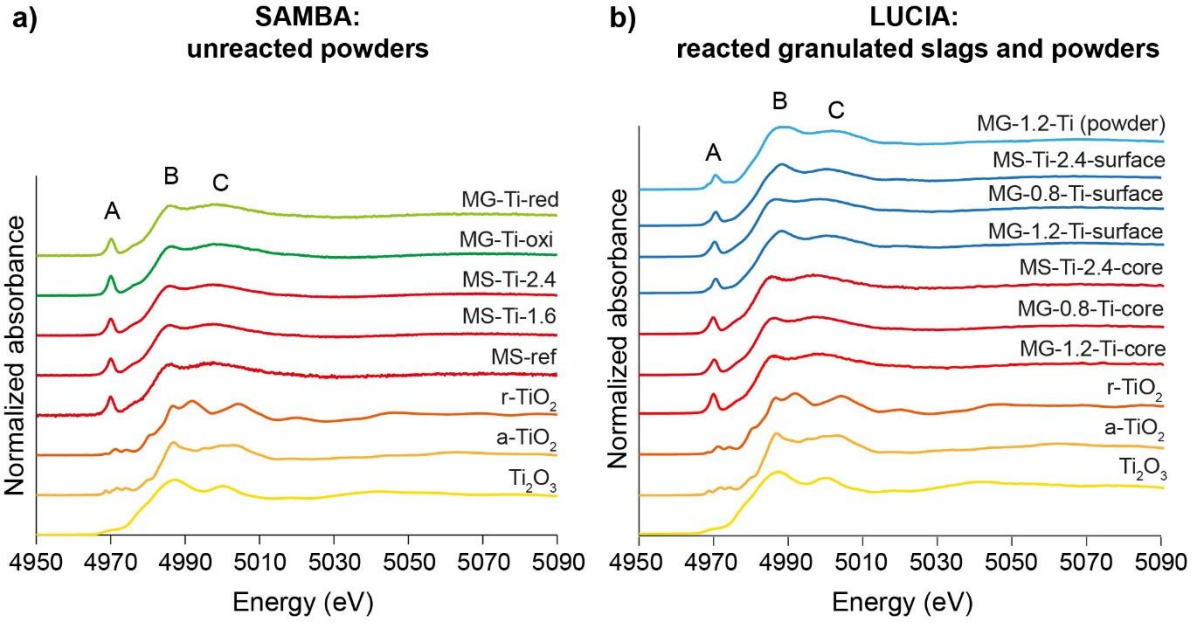

Figure 6. XANES spectra of Ti-modified GGBS, model glasses and mineral references collected at a) SAMBA and b) LUCIA. All samples show a single pre-edge peak A at around 4970.0 eV, and two post edge features B at about 4986 eV and C at about 4998 eV. Mineral references show more complex pre-peak features, in line with literature.[20,43]

The precise absolute positions and normalized height of peak A are shown in Table 4. These features were related to the coordination number (CN) of Ti^{4+} in various Ti-bearing minerals and glasses.[18–21,43] Peak positions and heights were also determined for mixing of different coordination states in one sample.[43] Plotting our samples into the mixing scheme proposed by Farges et al., 1997 (Figure 7, stars) showed that Ti was in $^{[4]}$Ti, $^{[5]}$Ti and $^{[6]}$Ti coordination states. This is consistent with another study on GGBS and slag-like glasses,[44] where a mixture of $^{[4]}$Ti and $^{[5]}$Ti with traces of $^{[6]}$Ti was reported. Note that rutile and anatase mineral references were correctly positioned in the $^{[6]}$Ti domain.

Table 4. Pre-edge absolute positions and normalized height of the GGBS samples and their references.

	ID	Position (eV)	Normalized height
SAMBA	Ti_2O_3	4969.4	0.08
	a-TiO_2	4971.6	0.15
	r-TiO_2	4971.2	0.13
	MS-ref	4970.0	0.40
	MS-Ti-1.6	4970.0	0.38
	MS-Ti-2.5	4970.0	0.40
	MG-Ti-oxi	4970.1	0.49
	MG-Ti-red	4970.1	0.42
LUCIA	Ti_2O_3	4969.6	0.06
	a-TiO_2	4971.6	0.13

	r-TiO_2	4971.2	0.15
	MG-1.2-Ti-core	4970.0	0.41
	MG-0.8-Ti-core	4970.1	0.32
	MS-Ti-2.5-core	4969.9	0.35
	MG-1.2-Ti-surface	4970.5	0.28
	MG-0.8-Ti-surface	4970.2	0.31
	MS-Ti-2.5-surface	4970.5	0.27
	MG-1.2-Ti (powder)	4970.6	0.27

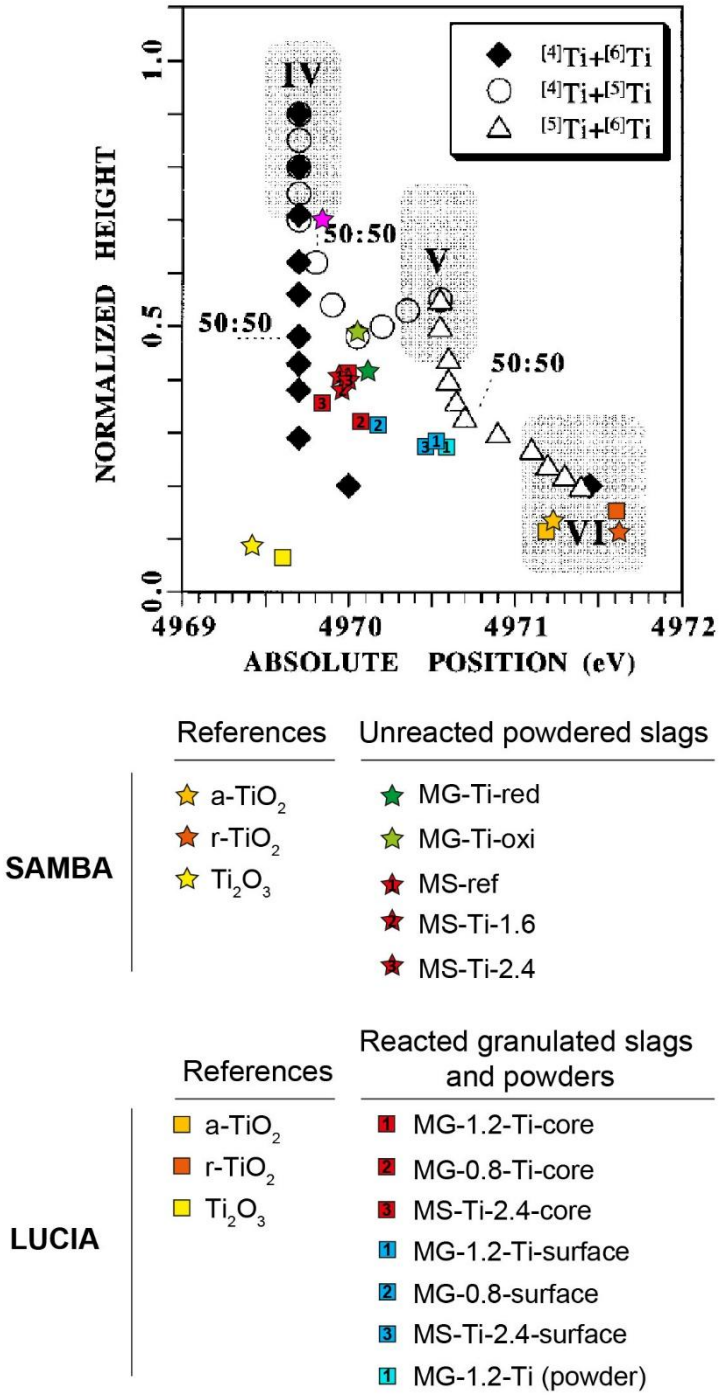

Figure 7. Pre-peak position and normalized height from Ti K-edge XANES, plotted in a diagram from literature to determine the coordination state of Ti(IV) species in the slag-glass samples and references compounds (modified from Farges et al., 1997).[43]

Besides CN, the pre-edge features can be influenced by the valence state of Ti.[45–47] Waychunas (1987) showed for example that the pre-peak position could shift by as much as -2.0 eV when the oxidation state decreased from Ti(IV) to Ti(III) in silicates and oxides with a similar chemical composition and a same coordination number.[46] Doyle et al., (2016), showed however, that in samples containing Ti(III) and Ti(IV) in the same coordination sites, the pre-peak position was only dependent on the coordination and the presence of Ti(III) only slightly lowered the pre-peak intensity.[48] A difference in pre-peak intensity of around 0.06, or 35% was detected between samples with 100% Ti(IV) (MG-Ti-oxi) and 100% Ti(III).[48] In our case, some variations in position and height can therefore be expected, especially as the slag-glass samples were prepared under reducing conditions that allow for the formation of Ti(III).

To rule out major misinterpretation of pre-edge features, two model glasses with slag-like composition prepared under oxidizing (MG-Ti-oxi) and reducing conditions (MG-Ti-red) were analyzed using XANES and EPR analyses. EPR analysis confirmed the presence of paramagnetic Ti(III) in MG-Ti-red produced under reducing conditions, showing a resonance at g=1.94 (H_R=360mT at 9.84GHz) (Figure SI-8).[44,49–51] In the oxidized model glass (MG-Ti-oxi) this resonance was not detected, showing the absence of Ti(III), as Ti(IV) cannot be detected by EPR due to its diamagnetic nature. Using the TiF_3 sample as reference, we estimated the a ratio of Ti(III)/ΣTi of 33% (+/-6%) in the MG-Ti-red sample. This value is close to the data reported for industrial GGBS with a proportion of 24% (+/-7.2%) Ti(III).[44] In XANES measurements the pre-edge position of Ti(III) containing sample (MG-Ti-red) fell into the same domain than the other slag samples. The normalized pre-peak height was slightly lower (-0.06 a.u) in the presence of Ti(III) than for the same sample containing exclusively Ti(IV) (MG-Ti-oxi). The presence of Ti(III) therefore may lead to an underestimation of the pre-edge peak intensity by -0.06 a.u in the slag-glass samples. The pre-peak position should not be affected. When pre-peak intensity was corrected for this relative decrease, all MG and MS samples fell into the domain of 70 % $^{[5]}$Ti and 30 % $^{[4]}$Ti, with only a minor contribution of $^{[6]}$Ti in slag glasses, in the diagram (Figure 7) proposed by Farges et al. (1997).[43]

3.3.2 Ti K-edge XANES analysis on reacted granulated slags and powdered samples (LUCIA)

The XANES spectra collected on the reacted slag samples are presented in Figure 6. The normalized heights and positions of the pre-edge peaks are summarized in Table 4. For the granulated slags exposed to pH 13, the analyses were carried out in the cores (intact glass) and at the surfaces (Ti-rich surface layer). The position of the measurement was specified in the sample names. For the powdered sample exposed to pH 11, only one measurement at the grain surface was reported.

The XANES spectra of the slag cores were similar to those of powdered GGBS measured at the SAMBA beamline: they were composed of a pre-edge at 4970 eV (peak A), and of two post-edge features at about 4986 eV (peak B) and 4998 eV (peak C). The intensity of peak C was slightly higher than that of peak B. Besides, there was a shoulder A' in the absorption edge at about 4976.5 eV (see Figure 8).

Figure 8 superposes the XANES spectra of the surface layers to their respective cores. In the surface layer, the pre-edge peak A shifted towards higher energies (~ 4970.5 eV) and had a lower intensity. The intensity of peak B was higher than that of peak C, while the inverse was true for the slag cores. According to the literature, peaks B and C are related to the medium-range structure around Ti.[20,43] Therefore, the structural organization around Ti was different between the unreacted slag cores and their reacted surface layers. The more pronounced oscillations in the surface layer indicates that the latter has a higher medium-range order than the unreacted slag. In MG-0.8-Ti, no difference was observed on the XANES spectra of the surface layer and slag core. This is probably due to the smaller size (3-10 µm) of the Ti-bearing layer in this sample, making it difficult to obtain an undisturbed surface layer signal.

The normalized heights and positions of the pre-peaks A were plotted in the mixing scheme of Farges et al., 1997 (Figure 7, squares). As for SAMBA, the anhydrous slag cores fell into the mixing domain of $^{[4]}$Ti +$^{[5]}$Ti +$^{[6]}$Ti. The pre-edge peak intensity was however potentially underestimated by 0.06 a.u due to the minor presence of Ti(III) in the samples (see section 3.3.1). Inter-sample variability in positions and intensity was higher, possibly due to the

different monochromators used in the two sessions (see Supporting Information, SI-3). Plotting the samples into the diagram (Figure 7) by Farges et al. (1997) resulted in about 50% of $^{[5]}$Ti and 50% of $^{[6]}$Ti.[43] The pre-peak position in XANES spectra of the surface layer of MG-1.2-Ti (powder), dissolved at pH 11 and MG-1.2-Ti-layer dissolved at pH 13 were identical. In addition, the features B and C were somewhat wider after dissolution at pH 11 than after dissolution at pH 13, but position and relative intensity were similar. Therefore, the coordination environment of Ti in the surface layer was independent of pH values during dissolution.

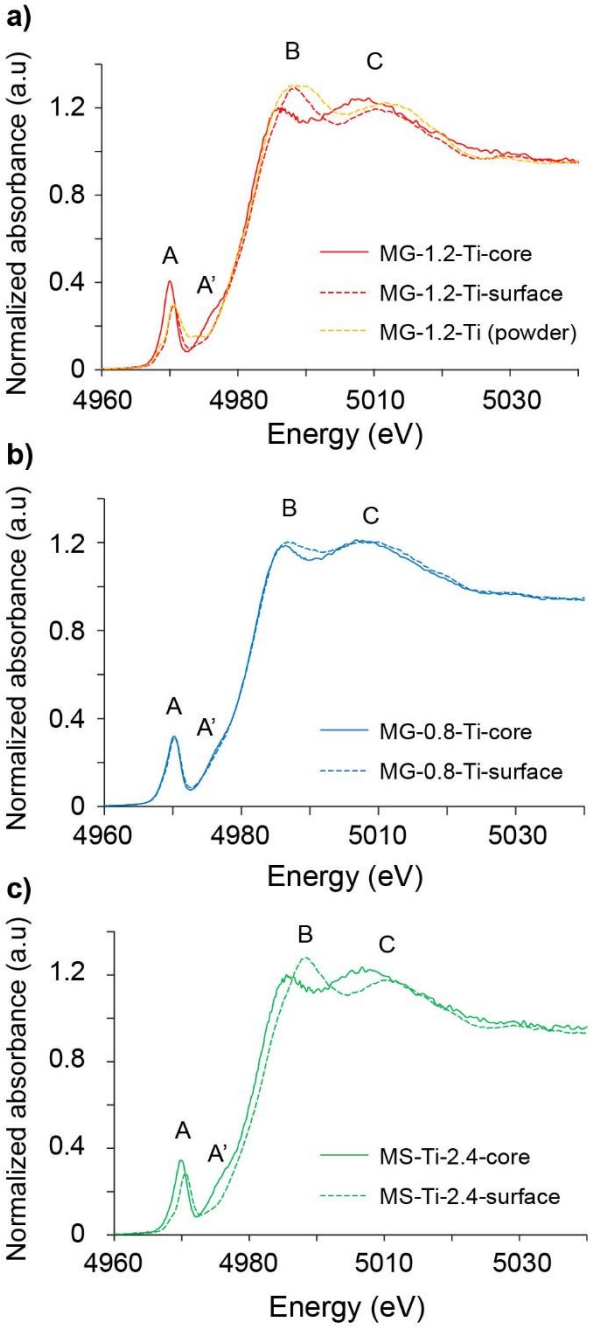

Figure 8: Comparison of the Ti K-edge XANES spectra of the slag core and surface layer of model glasses and modified slag samples.

3.4 Mg K-edge XANES measurements

Mg K-edge XANES spectra of the slag core and reacted surface of the granulated slag MG-1.2-Ti are presented in Figure 9. The XANES spectrum of the slag core was composed of four main features, located at about 1306.1 eV for a pre-edge peak P, 1309.2 eV and 1314.2 eV for two main features A and B, and 1326.0 eV for a broader peak C. Previous studies on Mg-bearing minerals and silicate glasses have attributed these features to various Mg environments.[52–56] The pre-edge peak P was assigned to a highly asymmetric environment of the first coordination shell. Peak A was related to the coordination number of Mg, as its position shifts towards higher energies when the coordination number increases from $^{[4]}$Mg (1307.2 eV) to $^{[8]}$Mg (1309.7 eV) in various Mg-bearing minerals. The $^{[5]}$Mg and $^{[6]}$Mg coordination states have intermediate energy positions between 1308.6 and 1309.3 eV, but cannot be differentiated because polyhedral distortion and multiple scattering influence the peak position. Peak B was related to the first coordination shell of Mg, while peak C was related to multiple scattering phenomena occurring within the outermost coordination shells around Mg. According to the energy position of peak A (1309.2 eV), the anhydrous slags contained Mg in five-fold and/or six-fold coordination. The low intensity of peak C indicates the absence of long range order around Mg, typical for glasses.

In contrast to the anhydrous slag, the reacted slag surface spectrum was composed of two well-defined features C’ (1317.9 eV) and D (1330 eV) in addition to the two main features A and B. No pre-edge peak P was present. The features C’ and D were related to multiple scattering phenomena occurring in the outermost coordination shells around Mg.[52,53] The higher intensity of the features C’ and D in the surface layer indicates a higher long-range order around Mg atoms than in the slag. The energy position of peak A (1310.9 eV) suggests a coordination >6 fold for Mg, however polyhedral distortions in the first coordination shell of Mg, or multiple scattering phenomena can increase the peak A position of $^{[6]}$Mg-bearing minerals above 1310 eV.[52,53] Altogether, the features A, B, C’ and D give a XANES spectrum very close to that of hydrotalcite.[57,58]

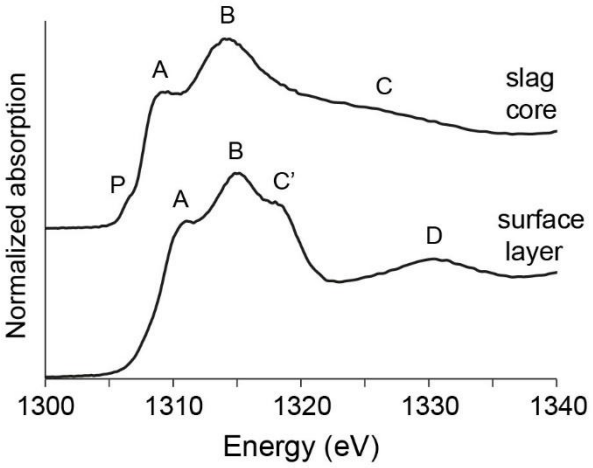

Figure 9: Mg K-edge XANES spectra of the slag core and reacted surface of the granulated slag MG-1.2-Ti.

4. Discussion

4.1 Ti and Mg in the slag structure

EPR analyses showed 67% of Ti(IV) and 33% of Ti(III) in the slag samples in line with existing literature.[17] After correction of pre-peak height for the presence of Ti(III), Ti K-edge XANES showed 70% of $^{[5]}$Ti and 30% of $^{[4]}$Ti coordination state, with a minor contribution of $^{[6]}$Ti. These results are in line with previous studies on industrial slags, alkali, alkaline-earth and borosilicate glasses.[17,18,22,42,43,47,59–64] The $^{[4]}$Ti coordination state corresponds to a tetrahedral geometry and $^{[5]}$Ti to a pyramidal geometry. In both cases, Ti integrates the alumino-silicate network of the slag glass.[17,59]

Mg K-edge XANES showed that Mg was mainly five-fold and/or six-fold coordinated in the slag structure. The local environment of Mg is highly asymmetric, and shows a low structural ordering at long distances. These results are consistent with previous studies on alumino-silicate glasses and slags, where Mg acts as a network modifier cation, mainly in 6-fold coordination.[14,52]

4.2 Dissolution rates of slag glasses at pH 11

Mixed-flow dissolution experiments at pH 11 and 20°C showed only a small impact of TiO_2 content on the dissolved Si masses (Figure 1). This was unexpected, since presence of Ti in slag glasses leads to a drastic decline of reactivity in cementitious settings, and initial dissolution rates were reported to significantly decrease for 4 mol% Ti (ca. 5 wt %) addition in a soda-lime borosilicate glass exposed to a pure water solution.[9,15,16,23,65] However, in our study, the pH during the dissolution trials was much higher (pH 11) and the Ti concentrations were well below (maximum of 1.9 mol%) those used in former Ti-bearing glass dissolution trials.[23] There was a clearer, but still small (about 10%), effect of Ti on the mean dissolution rates calculated for the first 48h of the dissolution experiments. The effect was somewhat stronger for the less polymerized MGs with 28 % slower dissolution of MG-0.8-Ti, compared to MG-0.8-NoTi. However, these rates were calculated making the hypothesis of spherical grain shape and homogeneous grain size, that cannot be verified with the present data.

The degree of polymerization of the glass network had a strong effect on dissolved glass masses. The more polymerized model glasses, MG-0.8-NoTi and MG-0.8-Ti, dissolved about a factor x 4 less within a week compared to the less polymerized homologues MG-1.2-NoTi and MG-1.2-Ti. The calculated initial dissolution rates were even a factor x 5-6 lower (Table 3). The lower Al and Si content of modified slags (MS-Ref and MS-Ti-2.5) further increased that difference. To be able to estimate the NBO/T value from composition for all glasses we propose to integrate TiO_2 into the formular as a network former (2). This is in line with the observations above, showing that Ti(IV) integrates the alumino-silicate network of slag-glasses. However, it does not represent an accurate structural description, because $^{[5]}$Ti possibly needs charge compensation and we do not have more precise information on the structural role of Ti(III), that represents about a third of Ti.[17,59]

$$\frac{\mathrm{NBO}}{\mathrm{T}}(\mathrm{Ti}) = \frac{2\mathrm{n_{Ca}} + 2\mathrm{n_{Mg}} - \mathrm{n_{Al}}}{\mathrm{n_{Si}} + \mathrm{n_{Al}} + \mathrm{n}_{Ti}} \qquad (2)$$

Plotting the NBO/T (Ti) values, estimated from glass composition, against dissolution rates calculated from Si release during the first 2 d of the experiment (Figure 10) shows all samples fell on the same regression line. This suggests that for the small compositional

variations investigated here, dissolution rates were correlated to the ratio of bridging to non-bridging oxygens and not by the nature of the network former ion. This is in line with research showing a strong control of the quantity of NBO on the initial glass dissolution rates.[11,66–68] However, the correlation may not be valid outside of the range of compositions investigated here, as the effects of NBO/T on dissolution rate have been reported to be non-linear, depending on the glass composition.[66,69] Changes in dissolution rate would also be expected according to the nature of the network forming ion (e.g. Si, Al, Ti). [11,23,26,69] This was not observed here, but was reported for other silicate glasses in literature.[23,66,69,70] The way Ti was taken into account in NBO/T (Ti) and the good correlation with dissolution rates implies that for the compositions investigated in this study the addition of a few percent of Ti did not change dissolution rates more than would an addition of the same amount of another network former (e.g. Si). This is in contrast to the strong negative effect of presence of a few weight percent of TiO_2 on the cementitious reactivity of slag glasses.[9,16,65]

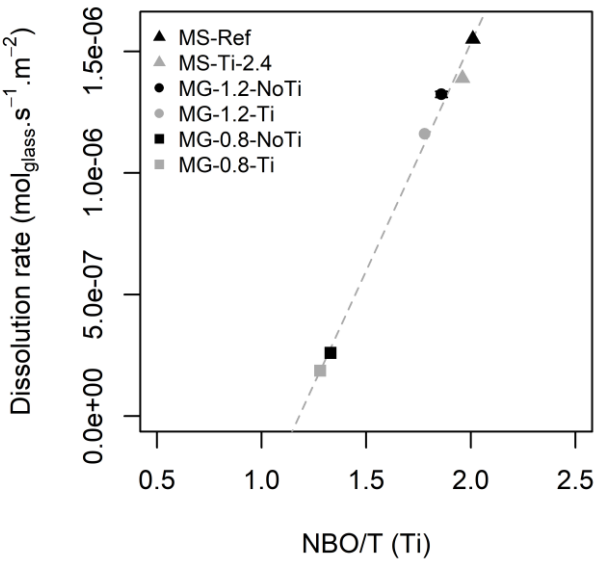

Figure 10. NBO/T (Ti) calculated from composition plotted against the mean dissolution rate, calculated from geometric surface area, during the first 2 d of the dissolution experiments at pH 11. The dashed line represents a linear regression computed on all samples. Two standard deviation error calculated from the replication of MG-1.2-NoTi is smaller that point.

Mixed-flow dissolution experiments at pH 11 and 20°C resulted in a mean dissolution rate of MS-Ref of 1.55 x 10^{-6} mol(glass).s^{-1}.m^{-2} during the first 48 h. This value is about one order of magnitude lower than that reported by Newlands et al. (2017) for the initial dissolution of slag-like model-glasses at pH 13 after half an hour of dissolution. The model glasses in that study contained no Mg and had relatively low NBO/T values of 1.1 (compared to 2.01 for MS-Ref), so that the increase in dissolution rate is due to the higher solution pH. Increasing pH values lead to stronger polarisation of Si-O bonds at the glass-solution interface and to thus higher hydrolysis rates.[11,24,67] The difference would probably be even larger for comparable polymerized glasses.

Steady state dissolution rates of slag like model glasses (NBO/T= 1.1, no Mg) by Snellings (2013) from batch dissolution experiments at pH 13 were one order of magnitude below the values reported here.[25] This difference might be explained by lower NBO/T values and relatively high solution concentrations in the batch experiments by Snellings 2013, that may have reduced their dissolution rates.

Dissolution of all samples was stoichiometric within the limits of experimental uncertainty for the main GGBS constituents Ca and Si. For some samples Mg and Al concentrations in solution were below the values expected for congruent dissolution, likely due to minor precipitation of Mg bearing phases such as hydrotalcite and brucite at high pH levels. Ti was not detected in solution even though its stoichiometric release should yield detectable Ti concentrations. Consequently, Ti may have precipitated or did not dissolve. An estimation of rutile solubility based on trials at 100°C shows that our solution should become oversaturated at a Ti concentration < 5 µg/L.[71] This concentration is close to the detection limit of the ICP-OES and would explain the non-detection of Ti in solution.

4.3 Surface layer formation

The formation of an alteration layer at the glass surface is commonly observed during aqueous dissolution of glass. In most cases the formation is attributed to recondensation of Si at the glass surface after leaching of more mobile network cations and precipitation of silica due to super-saturation of the attacking solution.[66] In this study, however, the surface

layer is mainly composed of Ti, only a minor constituent of the initial glass. Even though the presence of Ti, in the principally Si-alteration layer of a boro-silicate glass at pH 0 was already observed in literature, our observation is different as virtually no Si was present in the surface layer.[72] This may be due to the experimental design with high pH, leading to the dissolution of the alumino-silicate network and undersaturation with respect to amorphous silica.[73] Indeed, at pH 11, the surface layer was about 1 µm thick and contained mainly TiO_2 (66 wt.% TiO_2). At pH 13, the layer was larger (10 µm), probably due to higher glass network dissolution and TiO_2 (18.3 wt.% TiO_2) was accompanied by Mg and Al. The surface layer thickness appeared to be linked to the amount of glass alteration, as the thickness increased with pH and at the same pH was lower for MG-0.8-Ti, that dissolved slower, slower dissolution rates, than the other samples.

At both pH levels, the surface layer was amorphous to electron diffraction. Ti K-edge XANES showed that Ti recondensated at the slag-glass surface, with 50% of $^{[5]}$Ti and 50 % of $^{[6]}$Ti (against 70 % of $^{[5]}$Ti and 30 % of $^{[4]}$Ti in the unreacted slag). Furthermore, there was a higher medium-range order around Ti in the surface layer, compared to the slag. With the present data it is impossible to judge if this recondensation happens with or without complete dissolution of the TiO_2 units.

Ti K-edge XANES spectra of the surface layers were the same for both pH values. This observation suggests that Ti binding environment was identical in both conditions, so that Mg and Al in the surface layer are likely due to formation of a secondary phase and not bonded to Ti. This is supported by the fact that no common Ti-Mg-bearing minerals are reported in literature. The stoichiometric ratio of about 3 Mg : 1 Al, higher long-range order around Mg, similarity of the Mg-XANES spectrum and thermodynamic stability at high pH, suggest the formation of a hydrotalcite-like phase. This is in line with hydrotalcite precipitation at the slag surface during the hydration reaction.[74] Yet, this phase remained amorphous to electron diffraction, but hydrotalcite is often observed to be poorly crystalline in cement environments.[75] This observation highlights the possibility of secondary phase precipitation within the surface layer pores.

4.4 Implications for GGBS based cementitious materials

Presence of TiO_2 in GGBS glasses has a significant negative impact on the early age compressive strength of blended cements.[9,13,15,16,65] Compressive strength of MS-Ti-2.5 was reported to be 50 % below that of MS- Ref at 2 d and 28 d in standard mortars containing 75 wt.% of GGBS and 25 wt.% of ordinary Portland cement.[9] Earlier studies ascribed this loss to an increased strength of the glass network in the presence of Ti, resulting in lower dissolution rates.[9,17] Dissolution rate measurements reported here show small to not detectable differences dissolved Si masses in 7d experiments and TiO_2 contents similar or superior to former studies.[9,17] Even though Ti integrated the alumino-silicate network, these observations suggest that the drastic losses of reactivity are not only due to an increased stability of the glass network.

The presence of a Ti-bearing surface layer did not decrease the dissolution rate of slag glasses in the dissolution experiment. This implies that the surface layer was sufficiently porous to not significantly reduce diffusion of ions away from the glass surface into the bulk solution. In the literature, reduction of glass dissolution rates due to surface layer formation is commonly observed.[66,76,77] In a cement setting with concurrent dissolution and precipitation, the Ti surface layer might become passivating. The experiments at pH 13 suggest that Mg-aluminates, such as hydrotalcite, might precipitate in the pores. Under real cement conditions, precipitation of various hydrates in the Ti layer pores might reduce the diffusion up to the point at which the Ti layer passivates the glass surface, thus explaining drastic reactivity losses. This mechanism would be in line with significant losses of compressive strength only starting from 2-days for most TiO_2 contents, as the Ti layer would not form and become passivating immediately.[9]

5. Conclusions

The aim of this study was to investigate the role of Ti in the structure, dissolution rate and cementitious reactivity of GGBS-like glasses. It was shown that Ti integrates the alumino-silicate network in the slag glasses with 70 % in $^{[5]}$Ti and 30 % in $^{[4]}$Ti coordination state. Some 33% of Ti was present as Ti(III). The presence of Ti in the slag glasses had only a minor

(reduction of 10-28%) impact on initial dissolution rates at pH 11 and even less on dissolved Si after 7d. In contrast, calculated initial dissolution rates were found to be strongly affected by the degree of glass network polymerization and proportional to the NBO/T (Ti) ratio. During dissolution at pH 11 and pH 13 Ti accumulated in an amorphous phase at the slag glass surface. This layer contained 66 wt.% of TiO_2 at pH 11 and 18 wt.% at pH 13. The coordination environment of Ti in the layer increased from 70 % in $^{[5]}$Ti and 30 % in $^{[4]}$Ti in intact glass to 50% of $^{[5]}$Ti and 50% of $^{[6]}$Ti in the surface layer at both pH. At pH 13, the Ti-network was accompanied by Mg and Al likely in the form of poorly crystalline hydrotalcite. The Ti-rich surface layer did not reduce dissolution rates at pH 11. However, in a cement environment where hydrates precipitate the pores of the surface layer, this might be the case. Our results suggest that drastic reduced cementitious reactivity of GGBS in the presence of Ti is not only due to glass stabilization by network forming Ti but also by the formation of a Ti-rich surface layer with passivating properties, which protects the underlying surface against corrosion.

Acknowledgements

This project has received funding from the Research Fund for Coal and Steel, Ecocem and Arcelor-Mittal under grant agreement No 749809. The authors would like to thank Vanessa Mazars from the LMDC and Claudie Josse, Arnaud Proietti and Armel Descamps-Mandine from the Centre Raimond Castaing for help with electron microscopy. Furthermore, we thank Maud Schiettekatte for help with and maintenance of the ICP-OES.

Author contributions

SB and MP – performed all experiments except EPR analysis, carried out data analysis and conceptualization, and wrote the initial draft. DV and GL supervised XAS experiments at LUCIA (DV) and SAMBA (GL) and contributed to data analysis. EC, FF and VM contributed to conceptualization of results. CD and HV performed EPR measurements and data analysis. JK produced the samples, supervised the project and acquired funding. GS and JS, provided mixed flow reactors and supervised dissolution experiments. CP and MC contributed to conceptualization of results, acquired funding and supervised the project. All authors were involved in editing the manuscript.

References

(1) Ehrenberg, A. Huttensand - Ein Leistungsfahiger Baustoff Mit Tradition Und Zukunft - Teil 1. *Beton-Informationen* **2006**, *46* (4), 35–63.

(2) Matthes, W.; Vollpracht, A.; Villagrán, Y.; Kamali-Bernard, S.; Hooton, D.; Gruyaert, E.; Soutsos, M.; De Belie, N. Ground Granulated Blast-Furnace Slag. In *Properties of Fresh and Hardened Concrete Containing Supplementary Cementitious Materials*; De Belie, N., Soutsos, M., Gruyaert, E., Eds.; Springer International Publishing: Cham, 2018; Vol. 25, pp 1–53. https://doi.org/10.1007/978-3-319-70606-1_1.

(3) Bijen, J. Benefits of Slag and Fly Ash. *Construction and Building Materials* **1996**, *10* (5), 309–314. https://doi.org/10.1016/0950-0618(95)00014-3.

(4) Ehrenberg, A. CO2 Emissions and Energy Consumption of Granulated Blastfurnace Slag. In *Proceedings Manufacturing and Processing of Iron and Steel Slags*; Euroslag publication: Keyworth, UK, 2002; Vol. 3, pp 151–166.

(5) Hogan, F.; Meusel, J. Evaluation for Durability and Strength Development of a Ground Granulated Blast Furnace Slag. *Cement, Concrete and Aggregates* **1981**, *3* (1), 40. https://doi.org/10.1520/CCA10201J.

(6) Taylor, H. F. W. *Cement Chemistry*, 2nd ed.; Thomas Telford Publishing, 1997. https://doi.org/10.1680/cc.25929.

(7) Van den Heede, P.; De Belie, N. Environmental Impact and Life Cycle Assessment (LCA) of Traditional and 'Green' Concretes: Literature Review and Theoretical Calculations. *Cement and Concrete Composites* **2012**, *34* (4), 431–442. https://doi.org/10.1016/j.cemconcomp.2012.01.004.

(8) Blotevogel, S.; Ehrenberg, A.; Steger, L.; Doussang, L.; Kaknics, J.; Patapy, C.; Cyr, M. Ability of the R3 Test to Evaluate Differences in Early Age Reactivity of 16 Industrial Ground Granulated Blast Furnace Slags (GGBS). *Cement and Concrete Research* **2020**, *130*, 105998. https://doi.org/10.1016/j.cemconres.2020.105998.

(9) Blotevogel, S.; Steger, L.; Hart, D.; Doussang, L.; Kaknics, J.; Poirier, M.; Bornhöft, H.; Deubener, J.; Patapy, C.; Cyr, M. Effect of TiO_2 and 10 Minor Elements on the Reactivity of Ground Granulated Blast Furnace Slag (GGBS) in Blended Cements. *J Am Ceram Soc* **2020**, jace.17431. https://doi.org/10.1111/jace.17431.

(10) Blotevogel, S.; Montouillout, V.; Canizares, A.; Simon, P.; Chesneau, E.; Danezan, A.; Wattez, T.; Ehrenberg, A.; Poirier, M.; Patapy, C.; Cyr, M. Glass Structure of Industrial Ground Granulated Blast Furnace Slags (GGBS) Investigated by Time-Resolved Raman and NMR Spectroscopies. *J Mater Sci* **2021**, *56* (31), 17490–17504. https://doi.org/10.1007/s10853-021-06446-4.

(11) Bunker, B. C. Molecular Mechanisms for Corrosion of Silica and Silicate Glasses. *Journal of Non-Crystalline Solids* **1994**, *179*, 300–308. https://doi.org/10.1016/0022-3093(94)90708-0.

(12) Kucharczyk, S.; Sitarz, M.; Zajac, M.; Deja, J. The Effect of CaO/SiO 2 Molar Ratio of CaO-Al 2 O 3 -SiO 2 Glasses on Their Structure and Reactivity in Alkali Activated System. *Spectrochimica Acta Part A: Molecular and Biomolecular Spectroscopy* **2018**, *194*, 163–171. https://doi.org/10.1016/j.saa.2018.01.018.

(13) Smolczyk, H.-G. Zum Einfluß Der Chemie Des Hüttensands Auf Die Festigkeit von Hochofenzementen. *Zement - Kalk - Gips*. 6th ed. 1978, pp 294–296.

(14) Shimoda, K.; Tobu, Y.; Kanehashi, K.; Nemoto, T.; Saito, K. Total Understanding of the Local Structures of an Amorphous Slag: Perspective from Multi-Nuclear (29Si, 27Al, 17O, 25Mg, and 43Ca) Solid-State NMR. *Journal of Non-Crystalline Solids* **2008**, *354* (10–11), 1036–1043. https://doi.org/10.1016/j.jnoncrysol.2007.08.010.

(15) Ehrenberg, A. Huttensand - Ein Leistungsfahiger Baustoff Mit Tradition Und Zukunft - Teil 2. *Beton-Informationen* **2006**, *46* (5), 67–95.

(16) Wang, P. Z.; Rudert, V.; Lang, E.; Trettin, R. Influence of the TiO2 Content on the Reactivity of Granulated Blastfurnace Slags. *Cement Internationl* **2002**, *1*, 120–128.
(17) Le Cornec, D.; Galoisy, L.; Izoret, L.; Cormier, L.; Trcera, N.; Calas, G. Structural Role of Titanium on Slag Properties. *J. Am. Ceram. Soc.* **2021**, *104* (1), 105–113. https://doi.org/10.1111/jace.17407.
(18) Dingwell, D. B.; Paris, E.; Seifert, F.; Mottana, A.; Romano, C. X-Ray Absorption Study of Ti-Bearing Silicate Glasses. *Physics and Chemistry of Minerals* **1994**, *21* (8), 501–509. https://doi.org/10.1007/BF00203924.
(19) Farges, F. A Ti K-Edge EXAFS Study of the Medium Range Environment around Ti in Oxide Glasses. *Journal of Non-Crystalline Solids* **1999**, *244* (1), 25–33. https://doi.org/10.1016/S0022-3093(98)00846-1.
(20) Farges, F.; Brown, G. E.; Navrotsky, A.; Gan, H.; Rehr, J. J. Coordination Chemistry of Ti(IV) in Silicate Glasses and Melts: II. Glasses at Ambient Temperature and Pressure. *Geochimica et Cosmochimica Acta* **1996**, *60* (16), 3039–3053. https://doi.org/10.1016/0016-7037(96)00145-7.
(21) Romano, C.; Paris, E.; Poe, B. T.; Giuli, G.; Dingwell, D. B.; Mottana, A. Effect of Aluminum on Ti-Coordination in Silicate Glasses: A XANES Study. *American Mineralogist* **2000**, *85* (1), 108–117. https://doi.org/10.2138/am-2000-0112.
(22) Henderson, G.; Fleet, M. The Structure of Ti-Silicate Glasses by Micro-Raman Spectroscopy. *CANADIAN MINERALOGIST* **1995**, *33* (2), 399–408.
(23) Bergeron, B.; Galoisy, L.; Jollivet, P.; Angeli, F.; Charpentier, T.; Calas, G.; Gin, S. First Investigations of the Influence of IVB Elements (Ti, Zr, and Hf) on the Chemical Durability of Soda-Lime Borosilicate Glasses. *Journal of Non-Crystalline Solids* **2010**, *356* (44–49), 2315–2322. https://doi.org/10.1016/j.jnoncrysol.2010.07.065.
(24) Newlands, K. C.; Foss, M.; Matchei, T.; Skibsted, J.; Macphee, D. E. Early Stage Dissolution Characteristics of Aluminosilicate Glasses with Blast Furnace Slag- and Fly-Ash-like Compositions. *J Am Ceram Soc* **2017**, *100* (5), 1941–1955. https://doi.org/10.1111/jace.14716.
(25) Snellings, R. Solution-Controlled Dissolution of Supplementary Cementitious Material Glasses at PH 13: The Effect of Solution Composition on Glass Dissolution Rates. *Journal of the American Ceramic Society* **2013**, *96* (8), 2467–2475. https://doi.org/10.1111/jace.12480.
(26) Cailleteau, C.; Angeli, F.; Devreux, F.; Gin, S.; Jestin, J.; Jollivet, P.; Spalla, O. Insight into Silicate-Glass Corrosion Mechanisms. *Nature Materials* **2008**, *7*, 978.
(27) Gin, S. Open Scientific Questions about Nuclear Glass Corrosion. *Procedia Materials Science* **2014**, *7*, 163–171. https://doi.org/10.1016/j.mspro.2014.10.022.
(28) Gin, S.; Frugier, P.; Jollivet, P.; Bruguier, F.; Curti, E. New Insight into the Residual Rate of Borosilicate Glasses: Effect of S/V and Glass Composition. *Int J Appl Glass Sci* **2013**, *4* (4), 371–382. https://doi.org/10.1111/ijag.12048.
(29) Rahimi, R. A.; Sadrnezhaad, S. K. Effects of Ion-Exchange and Hydrolysis Mechanisms on Lead Silicate Glass Corrosion. *CORROSION* **2012**, *68* (9), 793–800. https://doi.org/10.5006/0528.
(30) Gunnarsson, I.; Arnórsson, S. Amorphous Silica Solubility and the Thermodynamic Properties of H4SiO°4 in the Range of 0° to 350°C at Psat. *Geochimica et Cosmochimica Acta* **2000**, *64* (13), 2295–2307. https://doi.org/10.1016/S0016-7037(99)00426-3.
(31) Jantzen, C. M.; Plodinec, M. J. Thermodynamic Model of Natural, Medieval and Nuclear Waste Glass Durability. *Journal of Non-Crystalline Solids* **1984**, *67* (1–3), 207–223. https://doi.org/10.1016/0022-3093(84)90151-0.
(32) O'Neill, H. St. C. Free Energy of Formation of Zircon and Hafnon. *American Mineralogist* **2006**, *91* (7), 1134–1141. https://doi.org/10.2138/am.2006.2071.
(33) Paul, A. Chemical Durability of Glasses; a Thermodynamic Approach. *J Mater Sci* **1977**, *12* (11), 2246–2268. https://doi.org/10.1007/BF00552247.
(34) Rimstidt, J. D.; Barnes, H. L. The Kinetics of Silica-Water Reactions. *Geochimica et Cosmochimica Acta* **1980**, *44* (11), 1683–1699. https://doi.org/10.1016/0016-7037(80)90220-3.

(35) Cailleteau, C.; Devreux, F.; Spalla, O.; Angeli, F.; Gin, S. Why Do Certain Glasses with a High Dissolution Rate Undergo a Low Degree of Corrosion? *The Journal of Physical Chemistry C* **2011**, *115* (13), 5846–5855. https://doi.org/10.1021/jp111458f.
(36) Brown, G. E.; Farges, F.; Calas, G. X-Ray Scattering and X-Ray Spectroscopy Studies of Silicate Melts. In *Rev. Mineral.*; Reviews in Mineralogy; Mineralogical Society of America: Washington D.C., 1995; Vol. 32, pp 317–410.
(37) Stebbins, J. F. Chapter 7. DYNAMICS AND STRUCTURE OF SILICATE AND OXIDE MELTS: NUCLEAR MAGNETIC RESONANCE STUDIES; Stebbins, J. F., McMillan, P. F., Dingwell, D. B., Eds.; De Gruyter, 1995; pp 191–246. https://doi.org/10.1515/9781501509384-009.
(38) Toplis, M. J.; Kohn, S. C.; Smith, M. E.; Poplett, I. J. F. Fivefold-Coordinated Aluminum in Tectosilicate Glasses Observed by Triple Quantum MAS NMR. *American Mineralogist* **2000**, *85* (10), 1556–1560. https://doi.org/10.2138/am-2000-1031.
(39) Neuville, D. R.; Cormier, L.; Massiot, D. Al Coordination and Speciation in Calcium Aluminosilicate Glasses: Effects of Composition Determined by 27Al MQ-MAS NMR and Raman Spectroscopy. *Chemical Geology* **2006**, *229* (1–3), 173–185. https://doi.org/10.1016/j.chemgeo.2006.01.019.
(40) Neuville, D. R.; Cormier, L.; Massiot, D. Al Environment in Tectosilicate and Peraluminous Glasses: A 27Al MQ-MAS NMR, Raman, and XANES Investigation. *Geochimica et Cosmochimica Acta* **2004**, *68* (24), 5071–5079. https://doi.org/10.1016/j.gca.2004.05.048.
(41) Ravel, B.; Newville, M. ATHENA and ARTEMIS Interactive Graphical Data Analysisusing IFEFFIT. *Physica Scripta* **2005**, 1007. https://doi.org/10.1238/Physica.Topical.115a01007.
(42) Cormier, L.; Dargaud, O.; Menguy, N.; Henderson, G. S.; Guignard, M.; Trcera, N.; Watts, B. Investigation of the Role of Nucleating Agents in $MgO{-}SiO_2{-}Al_2O_3{-}SiO_2{-}TiO_2$ Glasses and Glass-Ceramics: A XANES Study at the Ti K- and $L_{2,3}$ -Edges. *Crystal Growth & Design* **2011**, *11* (1), 311–319. https://doi.org/10.1021/cg101318p.
(43) Farges, F.; Brown, G. E.; Rehr, J. J. Ti K -Edge XANES Studies of Ti Coordination and Disorder in Oxide Compounds: Comparison between Theory and Experiment. *Phys. Rev. B* **1997**, *56* (4), 1809–1819. https://doi.org/10.1103/PhysRevB.56.1809.
(44) Le Cornec, D. Etude de La Structure Moléculaire Des Laitiers Vitrifiés de Hauts Fourneaux et de Leur Réactivité à l'eau En Milieu Basique. PhD-Thesis, Sorbonne Université, Paris, 2019.
(45) Ollier, N.; Lombard, P.; Farges, F.; Boizot, B. Titanium Reduction Processes in Oxide Glasses under Electronic Irradiation. *Journal of Non-Crystalline Solids* **2008**, *354* (2–9), 480–485. https://doi.org/10.1016/j.jnoncrysol.2007.07.078.
(46) Waychunas, G. A. Synchrotron Radiation XANES Spectroscopy of Ti in Minerals; Effects of Ti Bonding Distances, Ti Valence, and Site Geometry on Absorption Edge Structure. *American Mineralogist* **1987**, *72* (1–2), 89–101.
(47) Yang, X. C.; Dubiel, M.; Ehrt, D.; Schütz, A. X-Ray Absorption near Edge Structure Analysis of Valence State and Coordination Geometry of Ti Ions in Borosilicate Glasses. *Journal of Non-Crystalline Solids* **2008**, *354* (12–13), 1172–1174. https://doi.org/10.1016/j.jnoncrysol.2006.11.034.
(48) Doyle, P. M.; Berry, A. J.; Schofield, P. F.; Mosselmans, J. F. W. The Effect of Site Geometry, Ti Content and Ti Oxidation State on the Ti K-Edge XANES Spectrum of Synthetic Hibonite. *Geochimica et Cosmochimica Acta* **2016**, *187*, 294–310. https://doi.org/10.1016/j.gca.2016.05.001.
(49) Arafa, S.; Assabghy, F. Titanium Impurity Center Induced in Irradiated Silicate Glasses. *Journal of Applied Physics* **1974**, *45* (12), 5269–5271. https://doi.org/10.1063/1.1663228.
(50) Iwamoto, N.; Hidaka, H.; Makino, Y. State of Ti3+ Ion and Ti3+-Ti4+ Redox Reaction in Reduced Sodium Silicate Glasses. *Journal of Non-Crystalline Solids* **1983**, *58* (1), 131–141. https://doi.org/10.1016/0022-3093(83)90108-4.
(51) Lombard, P.; Ollier, N.; Boizot, B. EPR Study of Ti3+ Ions Formed under Beta Irradiation in Silicate Glasses. *Journal of Non-Crystalline Solids* **2011**, *357* (7), 1685–1689. https://doi.org/10.1016/j.jnoncrysol.2010.12.015.

(52) Trcera, N.; Cabaret, D.; Rossano, S.; Farges, F.; Flank, A.-M.; Lagarde, P. Experimental and Theoretical Study of the Structural Environment of Magnesium in Minerals and Silicate Glasses Using X-Ray Absorption near-Edge Structure. *Phys Chem Minerals* **2009**, *36* (5), 241–257. https://doi.org/10.1007/s00269-008-0273-z.

(53) Li, D.; Peng, M.; Murata, T. Coordination and Local Structure of Magnesium in Silicate Minerals and Glasses: Mg K-Edge XANES Study. *The Canadian Mineralogist* **1999**, *37*, 199–206.

(54) Ragoen, C.; Cormier, L.; Bidegaray, A.-I.; Vives, S.; Henneman, F.; Trcera, N.; Godet, S. A XANES Investigation of the Network-Modifier Cations Environment before and after the Na + /K + Ion-Exchange in Silicate Glasses. *Journal of Non-Crystalline Solids* **2018**, *479*, 97–104. https://doi.org/10.1016/j.jnoncrysol.2017.10.021.

(55) Morizet, Y.; Trcera, N.; Larre, C.; Rivoal, M.; Le Menn, E.; Vantelon, D.; Gaillard, F. X-Ray Absorption Spectroscopic Investigation of the Ca and Mg Environments in CO2-Bearing Silicate Glasses. *Chemical Geology* **2019**, *510*, 91–102. https://doi.org/10.1016/j.chemgeo.2019.02.014.

(56) Yoshimura, T.; Tamenori, Y.; Iwasaki, N.; Hasegawa, H.; Suzuki, A.; Kawahata, H. Magnesium K-Edge XANES Spectroscopy of Geological Standards. *J Synchrotron Rad* **2013**, *20* (5), 734–740. https://doi.org/10.1107/S0909049513016099.

(57) Vespa, M.; Dähn, R.; Huthwelker, T.; Wieland, E. Soft X-Ray Absorption near-Edge Investigations of Mg-Containing Mineral Phases Relevant for Cementitious Materials. *Physics and Chemistry of the Earth* **2017**, *99*, 168–174. http://dx.doi.org/10.1016/j.pce.2017.03.006.

(58) van Bokhoven, J. A.; Roelofs, J. C. A. A.; de Jong, K. P.; Koningsberger, D. C. Unique Structural Properties of the Mg-Al Hydrotalcite Solid Base Catalyst: An In Situ Study Using Mg and Al K-Edge XAFS during Calcination and Rehydration. *Chem. Eur. J.* **2001**, *7* (6), 1258–1265. https://doi.org/10.1002/1521-3765(20010316)7:6<1258::AID-CHEM1258>3.0.CO;2-I.

(59) Cormier, L.; Gaskell, P. H.; Calas, G.; Soper, A. K. Medium-Range Order around Titanium in a Silicate Glass Studied by Neutron Diffraction with Isotopic Substitution. *Phys. Rev. B* **1998**, *58* (17), 11322–11330. https://doi.org/10.1103/PhysRevB.58.11322.

(60) Paris, E.; Dingwell, D. B.; Seifert, F. A.; Mottana, A.; Romano, C. Pressure-Induced Coordination Change of Ti in Silicate Glass: A XANES Study. *Phys Chem Minerals* **1994**, *21* (8). https://doi.org/10.1007/BF00203925.

(61) Henderson, G. S. The Structure of Silicate Melts: A Glass Perspective. *The Canadian Mineralogist* **2005**, *43* (6), 1921–1958. https://doi.org/10.2113/gscanmin.43.6.1921.

(62) Henderson, G. S.; Liu, X.; Fleet, M. E. A Ti L -Edge X-Ray Absorption Study of Ti-Silicate Glasses. *Physics and Chemistry of Minerals* **2002**, *29* (1), 32–42. https://doi.org/10.1007/s002690100208.

(63) Yarker, C. A.; Johnson, P. A. V.; Wright, A. C.; Wong, J.; Greegor, R. B.; Lytle, F. W.; Sinclair, R. N. Neutron Diffraction and Exafs Evidence for TiO5 Units in Vitreous K2O · TiO2 · 2SiO2. *Journal of Non-Crystalline Solids* **1986**, *79* (1–2), 117–136. https://doi.org/10.1016/0022-3093(86)90041-4.

(64) Osipov, A. A.; Korinevskaya, G. G.; Osipova, L. M.; Muftakhov, V. A. Titanium Coordination in TiO2-Na2O-SiO2 Glasses of XTiO2 · (100 − x) [2Na2O · 3SiO2] (0 ≤ x ≤ 30) Composition Based on Raman Spectroscopy. *Glass Phys Chem* **2012**, *38* (4), 357–360. https://doi.org/10.1134/S1087659612040098.

(65) Tänzer, R.; Buchwald, A.; Stephan, D. Effect of Slag Chemistry on the Hydration of Alkali-Activated Blast-Furnace Slag. *Materials and Structures* **2015**, *48* (3), 629–641. https://doi.org/10.1617/s11527-014-0461-x.

(66) Gin, S.; Delaye, J.-M.; Angeli, F.; Schuller, S. Aqueous Alteration of Silicate Glass: State of Knowledge and Perspectives. *npj Mater Degrad* **2021**, *5* (1), 42. https://doi.org/10.1038/s41529-021-00190-5.

(67) Kerisit, S.; Ryan, J. V.; Pierce, E. M. Monte Carlo Simulations of the Corrosion of Aluminoborosilicate Glasses. *Journal of Non-Crystalline Solids* **2013**, *378*, 273–281. https://doi.org/10.1016/j.jnoncrysol.2013.07.014.

(68) Kerisit, S.; Pierce, E. M. Monte Carlo Simulations of the Dissolution of Borosilicate and Aluminoborosilicate Glasses in Dilute Aqueous Solutions. *Geochimica et Cosmochimica Acta* **2011**, *75* (18), 5296–5309. https://doi.org/10.1016/j.gca.2011.06.036.
(69) Damodaran, K.; Delaye, J.-M.; Kalinichev, A. G.; Gin, S. Deciphering the Non-Linear Impact of Al on Chemical Durability of Silicate Glass. *Acta Materialia* **2021**, 117478. https://doi.org/10.1016/j.actamat.2021.117478.
(70) Wolff-Boenisch, D.; Gislason, S. R.; Oelkers, E. H.; Putnis, C. V. The Dissolution Rates of Natural Glasses as a Function of Their Composition at PH 4 and 10.6, and Temperatures from 25 to 74°C. *Geochimica et Cosmochimica Acta* **2004**, *68* (23), 4843–4858. https://doi.org/10.1016/j.gca.2004.05.027.
(71) Knauss, K. G.; Dibley, M. J.; Bourcier, W. L.; Shaw, H. F. Ti(IV) Hydrolysis Constants Derived from Rutile Solubility Measurements Made from 100 to 300°C. *Applied Geochemistry* **2001**, *16* (9–10), 1115–1128. https://doi.org/10.1016/S0883-2927(00)00081-0.
(72) Geisler, T.; Janssen, A.; Scheiter, D.; Stephan, T.; Berndt, J.; Putnis, A. Aqueous Corrosion of Borosilicate Glass under Acidic Conditions: A New Corrosion Mechanism. *Journal of Non-Crystalline Solids* **2010**, *356* (28–30), 1458–1465. https://doi.org/10.1016/j.jnoncrysol.2010.04.033.
(73) Perez, A.; Daval, D.; Fournier, M.; Vital, M.; Delaye, J.-M.; Gin, S. Comparing the Reactivity of Glasses with Their Crystalline Equivalents: The Case Study of Plagioclase Feldspar. *Geochimica et Cosmochimica Acta* **2019**, *254*, 122–141. https://doi.org/10.1016/j.gca.2019.03.030.
(74) Li, B.; Li, Q.; Chen, W. Spatial Zonation of a Hydrotalcite-like Phase in the Inner Product of Slag: New Insights into the Hydration Mechanism. *Cement and Concrete Research* **2021**, *145*, 106460. https://doi.org/10.1016/j.cemconres.2021.106460.
(75) Bernard, E.; Zucha, W. J.; Lothenbach, B.; Mäder, U. Stability of Hydrotalcite (Mg-Al Layered Double Hydroxide) in Presence of Different Anions. *Cement and Concrete Research* **2022**, *152*, 106674. https://doi.org/10.1016/j.cemconres.2021.106674.
(76) Gin, S.; Beaudoux, X.; Angéli, F.; Jégou, C.; Godon, N. Effect of Composition on the Short-Term and Long-Term Dissolution Rates of Ten Borosilicate Glasses of Increasing Complexity from 3 to 30 Oxides. *Journal of Non-Crystalline Solids* **2012**, *358* (18–19), 2559–2570. https://doi.org/10.1016/j.jnoncrysol.2012.05.024.
(77) Ferrand, K.; Klinkenberg, M.; Caes, S.; Poonoosamy, J.; Van Renterghem, W.; Barthel, J.; Lemmens, K.; Bosbach, D.; Brandt, F. Dissolution Kinetics of International Simple Glass and Formation of Secondary Phases at Very High Surface Area to Solution Ratio in Young Cement Water. *Materials* **2021**, *14* (5), 1254. https://doi.org/10.3390/ma14051254.